Materials Today Communications 50 (2026) 114387

Contents lists available at ScienceDirect

Materials Today Communications

journal homepage: www.elsevier.com/locate/mtcomm

Machinability analysis of Inconel 718 through parametric optimization using novel laser hybrid micro milling technique

Ahmad Waqar Tehami [a], Muhammad Rizwan ul Haq [a], Muhammad Ali Khan [a,b,*], Syed Husain Imran Jaffery [a,c,**], Muhammad Iftikhar Faraz [d], Jana Petru [e]

[a] School of Mechanical and Manufacturing Engineering (SMME), National University of Sciences and Technology (NUST), Islamabad 44000, Pakistan
[b] Department of Mechanical Engineering, College of Electrical and Mechanical Engineering (CEME), National University of Sciences and Technology (NUST), Islamabad 44000, Pakistan
[c] Department of Mechanical Engineering, College of Engineering, Faculty of Computing, Engineering and the Built Environment Birmingham City University, Birmingham B4 7XG, UK
[d] Department of Mechanical Engineering, College of Engineering, King Faisal University, Al-Ahsa, Saudi Arabia
[e] Department of Machining, Assembly and Engineering Metrology, Mechanical Engineering Faculty, VSB-Technical University of Ostrava, 17, Listopadu 2172/15, Ostrava 708 00, Czech Republic

ARTICLE INFO

Keywords:
Laser Hybrid Micromachining
Micromilling
Inconel 718 Superalloy
Multi-objective Optimization
Analysis of Variance
Grey Relational Analysis
Response Surface Methodology

ABSTRACT

Miniaturization is reshaping the landscape of advanced manufacturing to fulfil the demands of micro components with exceptional precision and functionality in sectors such as aerospace, biomedical and microelectronics. Hybrid techniques syndicate distinct machining processes to leverage their unique benefits while minimizing inherent limitations. This experimental study proposes a novel laser hybrid micro milling technique intended to synergize laser assistance with mechanical micro milling. To explore the machinability of Inconel 718, experiments were designed at feed rates below, at and above the cutting-edge radius with uncoated and three different coated tools using Taguchi L-16 orthogonal array. Cutting speed, feed rate, depth of cut and tool type, each evaluated across four discrete levels to analyze their impact on critical responses: surface roughness, tool wear and burr formation. Analysis of Variance (ANOVA) and Grey Relational Analysis (GRA) were employed to evaluate the significance of each parameter and to determine the optimal combination of variables. Uncoated tools yielded the lowest roughness and tool wear, TiAlN coatings minimized burrs. ANOVA of the regression model revealed the tool type as the most influencing factor with 73.68 % contribution. GRA identified 9 m/min speed, 2.5 μm/tooth feed and 60 μm cutting depth with TiAlN coated tool as optimal run. Optimization using Response Surface Methodology (RSM) led to 23.08 %, 24.04 % and 23.64 % average reduction in roughness, tool wear and burr formation, respectively, demonstrating the efficacy of the optimized process settings. The investigation significantly contributes by revealing parameter interactions and their impacts on burr mitigation, tool longevity, and surface quality.

1. Introduction

Miniaturization is the backbone of cutting-edge technological advancements, driven by the demand for small-scale, efficient and cost-effective solutions. It enhances device functionality in sectors like aerospace, automotive, biomedical and electronics by reducing size and creating space for additional features [1]. This trend fosters technological innovation, pushing the development of high-precision micro-components, typically made from hard-to-machine materials [2, 3]. Macro-machining has extensively been studied for decades but transitioning to the micro domain is more complex than merely scaling down macro features. Understanding the technical intricacies of micro-machining requires in-depth research [4]. High-stress, high-temperature and corrosive environments vigorously demand robust

* Corresponding author at: Department of Mechanical Engineering, College of Electrical and Mechanical Engineering (CEME), National University of Sciences and Technology (NUST), Islamabad 44000, Pakistan.
** Corresponding author at: School of Mechanical and Manufacturing Engineering (SMME), National University of Sciences and Technology (NUST), Islamabad 44000, Pakistan.
E-mail addresses: mak.ceme@ceme.nust.edu.pk (M.A. Khan), imran@smme.edu.pk (S.H.I. Jaffery).

https://doi.org/10.1016/j.mtcomm.2025.114387
Received 3 September 2025; Received in revised form 6 November 2025; Accepted 22 November 2025
Available online 23 November 2025
2352-4928/© 2025 The Author(s). Published by Elsevier Ltd. This is an open access article under the CC BY-NC-ND license (http://creativecommons.org/licenses/by-nc-nd/4.0/).

superalloys [5]. Nickel-based alloys are essential for components in aircraft, rockets and submarine engines operating at 450–700°C [6]. Inconel 718 stands out for its exceptional strength at high-temperature, resistance to corrosion and oxidation ensuring structural integrity under extreme conditions [7–9]. Its versatility makes it indispensable in aerospace for turbine blades, engine casings, combustion chambers and in automotive exhaust systems and high-performance engine parts [10, 11]. Due to its excellent resistance to heat and corrosion, it is preferred choice in sectors such as power generation, gas turbines and nuclear energy systems [12,13]. Inconel 718 is frequently alloyed with aluminum to produce lightweight and heat-resistant structural components [14,15]. The exceptional properties of nickel-based superalloys also contribute to their poor machinability, causing poor surface quality, significant tool wear and burr formation which require optimized machining parameters [16,17]. Key parameters like cutting speed, feed rate, tool diameter and tool coatings significantly influence the response variables. Tool wear is largely caused by cutting speeds at all levels [18]. Burr formation remains a critical issue, particularly in micro-machining, where small burrs complicate deburring processes and risk damaging delicate micro-features. While low-temperature pre-cooling suppresses burrs, it increases tool wear [19].

Among the various strategies, tool coatings have proven to be a highly effective method for overcoming machining difficulties. Irfan et al. [20,21] examined in their study how different coatings affected tool wear and roughness of Inconel 718 in high speed micromachining. He found that TiAlN+WC and Diamond Like Coatings function exceptionally well followed by AlTiN coated tools. Diamond tools with their exceptional hardness and wear resistance, are ideal for machining hard materials like Inconel 718 but are costly [22]. Alternatives include Si_3N_4 ceramic tools which leverage temperature-softening effects for efficiency, tungsten carbide tools with advanced coatings for versatility and Cubic Boron Nitrides (CBNs) though these catastrophically fail beyond certain cutting speed in machining of Inconel 718 [23]. Composite tools integrate different materials like diamond for its cutting power and carbide for toughness, offer a balanced approach [22,24–26]. This study compared the performance of uncoated tools with three coated variants: Titanium Aluminum Nitride (TiAlN), Titanium Silicon Nitride (TiSiN) and an AlTiSi-based nanocomposite (nACo). TiAlN, TiSiN and nACo coated tools were selected due to their established use in recent micromilling studies and their distinct mechanical/thermal advantages [27–29]. TiAlN provides high hardness and oxidation resistance, TiSiN offers further improved hardness and thermal stability due to its Si-based nanocomposite structure, while nACo shows the highest hardness and oxidation resistance among all three. These pronounced property differences make this coating set directly suitable for assessing coating-dependent performance in the present hybrid micromilling work.

Micromachining techniques face limitations despite extensive research, prompting the adoption of hybrid machining methods [30]. These methods combine two or more conventional or non-conventional processes, either in an assisted or sequential manner, leveraging multiple energy sources to enhance machining performance [31]. By combining different machining principles, hybrid processes amplify advantages and mitigate limitations, offering superior performance compared to individual techniques [32]. Hybrid micromachining, combining multiple techniques, achieves high precision and accuracy for micro-scale components. Techniques such as laser-assisted, vibration-assisted and machining with hybrid cooling or cryogenic environments have been developed to address machining challenges of nickel and titanium-based superalloys [33,34]. Hybrid techniques are novel and primarily used for fabricating micro-sized components in challenging materials. Non-traditional energy-assisted mechanical machining which integrates energies like vibration, laser and electricity while taking into account the structural and processing properties of components to enhance material machinability while reducing the mechanical burden [35]. Research by B. Lauwers et al. [36] reflects the advantage of combining conventional machining with laser processes. Softening of material through thermal energy of the laser substantially reduces cutting forces and torque.

Laser Beam Machining (LBM) is a versatile energy field machining technique that employs high-power laser pulses for material ablation and microfabrication. It is widely used for machining alloys, metals and ceramics. LBM achieves material ablation through focused beam energy, which transforms the substrate into molten, vaporized or chemically degraded states when the laser fluence exceeds the material's threshold, achieving precision at micron or sub-micron levels [37]. Innovations such as Laser-induced surface damage assisted machining enhance machinability by reducing cutting forces [38]. Investigations highlight that incorporating laser ablation into before micro-milling processes can significantly enhance performance. This approach results in a reduction in chip thickness through partial material removal ahead of milling which in turn lowers the cutting forces involved. Microhardness evaluations reveal that laser ablation can lead to a 30 % decrease in the material's strength [39]. A variety of laser types including gas, fiber and Nd:YAG lasers are used, depending on the required wavelength and energy output. J. P. Davim [40] states that fiber lasers are commonly employed for applications like surface cleaning and low intensity material removal. The adoption of lasers in modern manufacturing has opened up new opportunities particularly in aerospace and nuclear. C. A. McNally, J. Dutta Majumdar and I. Manna [41,42] have highlighted several limitations in addition to burrs and spatter such as tapering and poor circularity despite the fact that LBM provides rapid processing speed, capability to produce microscopic features and suitability for mass production. The constraints of LBM, such as unregulated dimensions and tapered surfaces, prevent it from producing finished products suitable for diverse applications [43]. Laser Assisted Machining (LAM) improves machinability by locally softening or altering material with a laser beam to create a metamorphic layer while mechanical machining eliminates the heat-affected zone [35]. Research of H. Zhang et al. [44] on laser-assisted micro-milling of Inconel 718 shows a moderate decrease in cutting forces.

Despite extensive research has been done to investigate the significance of machining parameters for the output responses like surface roughness, tool wear and burr formation during micromachining of superalloys but still a significant gap exists in the exploration of hybrid machining techniques that combine laser and mechanical micromachining in a sequential manner. Specifically, there is insufficient research that investigates the synergistic effects of these hybrid processes, coupled with various tool coatings and feed rates below, at and above cutting-edge radius. The selected feed per tooth values were chosen to distinguish the three micromilling regimes: ploughing, transition, and shearing. This design allows investigation of the coating and tool performance under both size-effect dominated and conventional cutting conditions, following the methodology adopted in prior micromilling studies done by Aramcharoen and Mativenga [45], de Oliveira et al. [46], Anand-Krishnan & Mathew [47] and Jaffery et al. [48]. Laser hybrid micro-milling has emerged as a cutting-edge technique capable of fabricating intricate freeform surfaces. Its integration with additional hybrid processes holds strong potential for resolving persistent issues in precision manufacturing [49]. Sequential hybrid machining, where different processes are employed one after the other, provides distinctive benefits by compensating for the shortcomings of individual methods. This results in enhanced surface integrity, dimensional accuracy and overall efficiency. Despite extensive research on laser-assisted micro-milling, the domain of sequential laser hybrid micro-milling remains relatively unexplored, presenting a lot of potential for technological advancements.

The experimental investigation presented in this study introduces an innovative sequential hybrid approach that advances the micro-scale machinability of Inconel 718. Although extensive work exists on parameter optimization for conventional micromachining of superalloys, a significant gap remains regarding hybrid strategies that combine

laser pre-machining with subsequent mechanical micro-milling. The capability of Laser Beam Machining (LBM) to create complex geometries without direct tool interaction or associated wear is joined with advantages found in mechanical machining, including high accuracy, operational flexibility, minimal thermal effects, lower tool consumption and environmentally sustainable processes. In particular, the synergistic effects of sequential laser–mechanical coupling together with different tool coatings and feed regimes below, at, and above the cutting-edge radius have not been comprehensively explored. Laser hybrid micro-milling has recently been recognized as an emerging technique with the potential to improve surface integrity and dimensional precision; however, the specific domain of sequential laser hybrid micro-milling remains under-reported. Therefore, this work addresses this research gap by implementing laser processing as a preliminary step followed by mechanical micromilling, and by systematically investigating the influence of machining parameters (spindle speed, feed rate and depth of cut) on surface roughness, tool wear and burr formation. This provides new insight into how coating type and scale-dependent feed levels influence performance in a sequential hybrid configuration. An optimal set of input parameters was established through multi-objective parametric optimization while the overall performance is quantified through an integrated Taguchi–ANOVA–GRA–RSM framework and verified through confirmatory tests.

2. Materials and methods

This research involved an experimental study on a combined machining technique that merges two different processes. This technique used a two-phase process. In the first phase, a fiber laser was used to create pilot slots. In the second step, the final geometry was achieved by mechanically micromilling these laser-generated pilot slots. Fiber lasers are highly versatile and cut through a variety of materials with precision. Mechanical machining processes handle materials that might be challenging for lasers alone. The laser efficiently handles the initial rough cutting. Mechanical machining allows for the refinement of these features to realize the desired surface quality and precise dimensions by ensuring tight tolerances and relieving thermal stresses induced by the laser process. The scheme of experimentation with subsequent analysis framework is illustrated in Fig. 1.

Speed, feed, and cutting depth are among the machining parameters that are systematically assessed using the Taguchi L-16 experimental design. Both coated (TiAlN, TiSiN, nACo) and uncoated cutting tools are evaluated to see how they affect response variables. A multi-objective optimization framework using RSM and GRA enhances the machining process by identifying the best parameter settings. The most favorable and least favorable machining parameters are determined by counting the influence of each individual element separately using ANOVA and regression modeling. Finally, validation trials authenticate the optimized parameters, guaranteeing the machining process's dependability and repeatability for high-precision applications.

2.1. Material selection

Inconel 718, a remarkable nickel-based alloy, has emerged as a game changer in the realm of engineering, offering unparalleled performance characteristics that have led to widespread adoption in diverse sectors. Inconel 718 is widely favored in demanding environments where traditional materials like steel and aluminum are unable to endure extreme conditions. While conventional alloys tend to degrade in high-temperature or corrosive settings, Inconel 718 retains its mechanical strength across a wide temperature spectrum. It is highly valued for its superior strength, resistance to corrosion and oxidation and excellent fatigue life, performing reliably at temperatures between 450°C and 700°C. This property makes it particularly suitable for manufacturing turbine blades used in high-pressure, high-temperature aero engines, engine casings, exhaust systems and nuclear reactors. It is preferred by aerospace, automotive, power generation and military industries [50–52].

Table 1 displays the mechanical characteristics of Inconel 718 [53] while Table 2 outlines the compositional breakdown of the material [54].

2.2. Cutting tool specifications

E. O. Ezugwu et al. [55] highlighted that for effective machining of nickel-based alloys, cutting tools must possess high levels of wear resistance, hot hardness, toughness, strength and thermal chemical stability. When dealing with micro-milling of Inconel 718, it becomes essential to evaluate the tool material considering its physical properties, machining environment and structural design. Due to its abrasive texture and capability to withstand high temperatures, Inconel 718 tends to cause rapid deterioration of tools under extreme thermal and mechanical loads [12,56–59]. According to findings by M. Takács et al. [60], the processing of materials previously regarded as difficult-to-machine have become more feasible. Enhanced machinability is attributed to key coating characteristics such as reduced friction, increased surface hardness and improved thermal resistance. These properties collectively contribute to extended tool life, lowered machining expenses and enhanced quality of the final product [26,59].

To improve chip evacuation during micro-milling, literature recommends using tools with wider spacing between cutting edges [61,62]. In line with this, a two-flute micro-milling cutter was selected, as it contributes to reduced torque and power requirements during the machining process. Micro-milling was executed on pre-generated pilot slots formed by laser machining, utilizing 500 μm diameter tungsten carbide end mills featuring two flutes and a 30° helix angle.

Fig. 2 illustrates the cutting tools employed in the study, while detailed specifications of both tools and coatings, sourced from North Carbide Tools, are presented in Table 3 and Table 4, respectively. The cutting-edge radius was measured using DSX-1000 Olympus Digital Microscope. The tool was positioned vertically, and the edge was focused at required magnification for precise imaging as shown in Fig. 2 (e). The radius was subsequently measured using the microscope's built-in measurement software. The cutting-edge radii were found to be 2.39 μm (uncoated), 2.53 μm (TiAlN), 2.82 μm (TiSiN), and 2.91 μm (nACo). Each experiment employed a fresh tool to eliminate variability due to wear.

2.3. Workpiece preparation

An Inconel 718 specimen with dimensions of 10 × 10 × 50 mm was securely mounted in a vice, and its top surface was precisely flattened using a 12 mm carbide square end mill to establish a reference plane. This reference surface was then utilized for subsequent laser-based pilot slot fabrication. The workpiece material was procured in 50 × 50 × 10 mm form, and machining was performed along the 10 mm thickness face. The required specimen size was prepared using an EDM wire-cutting machine to ensure precise dimensions and proper clamping in the precision vice. The material condition received is shown in Fig. 3(a). Without disturbing the clamping arrangement, the workpiece was then shifted to a micro-milling center to carry out the mechanical micromachining process. The precision vice ensured that the same center was maintained for both laser and conventional micro-milling operations. The laser-generated slot served as a reference feature for alignment of micro-tools using offset settings to ensure accurate centering. The experimental procedure involved machining slots with a length of 10 mm, maintaining a uniform spacing of 3 mm between adjacent slots, as depicted in Fig. 3(b).

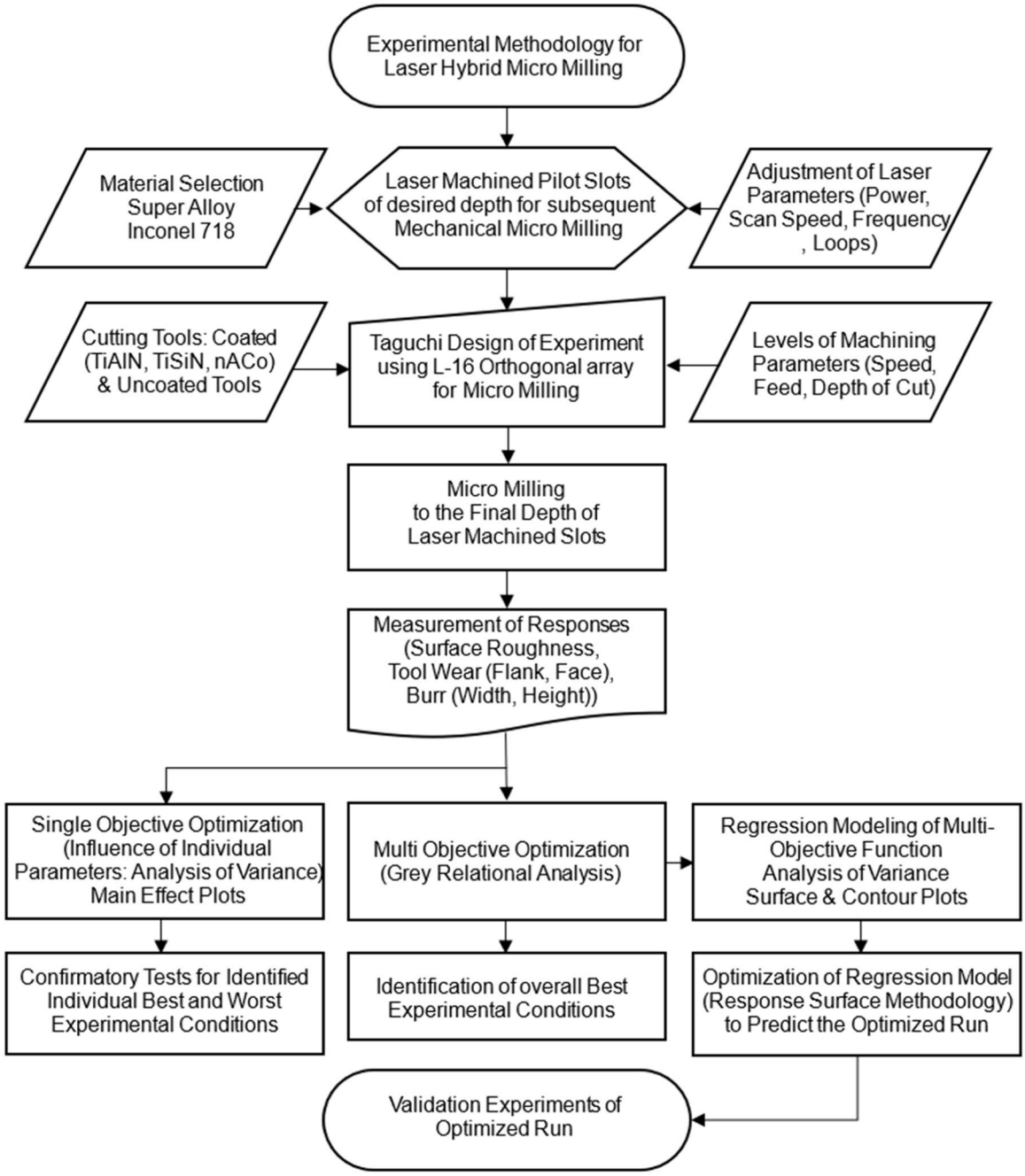

Fig. 1. Scheme of experimentation, measurement and subsequent analysis.

Table 1
Mechanical properties of Inconel 718.

Density (g/cm^3)	Hardness (HB)	Tensile Strength (MPa)	Elastic Modulus (GPa)	Thermal Conductivity (W/m.K)
8.2	390	1600	205	11.4

2.4. Laser engraving machine

In the first stage of the process, pilot slots were produced on the pre-processed workpiece surface using a fiber laser system (Raycus/IPG optional), developed by Maxphotonics as illustrated in Fig. 4. The operational parameters of the system including laser power, frequency

Table 2
Composition of Inconel 718 alloy (wt%).

Element	Ni	Fe	Cr	Nb	Mo	Ti	Al	C	S	Cu
Percentage	53.12	18.6	17.7	4.79	3.07	0.86	0.60	0.04	0.03	0.02

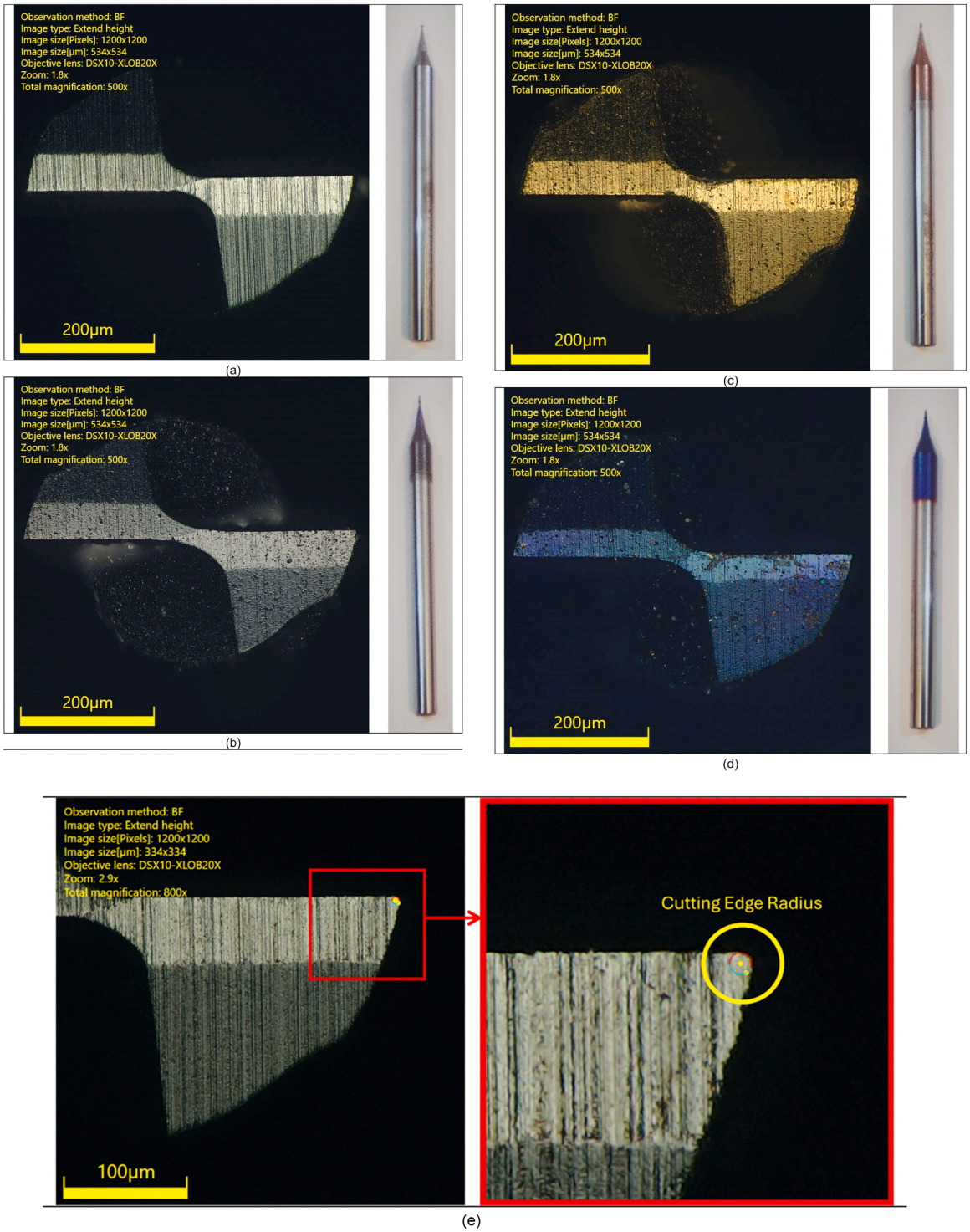

Fig. 2. Coated and uncoated Tools: (a) Uncoated; (b) TiAlN; (c) TiSiN; (d) nACo; (e) Cutting edge radius measurement.

Table 3
Details and specifications of cutting tool.

Specifications	Details
Material	Tungsten carbide
Brand name	North Carbide Tools
Type	Square End Carbide Mill
Overall length (mm)	50
Rockwell hardness (HRC)	60
Helix angle (o)	30

Table 4
Specifications of coatings.

Specification	AlTiN	TiSiN	nACo
Hardness (HV)	3200	3600	4500
Thickness (microns)	2.5–3	3	3
Oxidation temp (oC)	900	1000	1200
Coefficient of Friction	0.3	0.45	0.4
Color	Black	Golden	Blue

and scanning speed were precisely controlled through the Ezcad2 software's Graphical User Interface (GUI) allowing for a maximum achievable depth of 0.5 mm.

Detailed specifications and configuration settings of the laser equipment are provided in Table 5. This parameter-driven control strategy aligns with emerging trends in precision laser micromachining for high-performance alloys.

The finalized set of input parameters comprising laser power, frequency, number of loops and scanning speed was derived from an initial parametric analysis designed to attain a precise pilot slot depth. The preliminary depth was deliberately set 10 μm shallower than that of the final machined slot to ensure precision and process control. The pilot slots along with their corresponding process parameters are presented in Fig. 5.

2.5. Milling machine

After generating pilot slots, work-piece was then machined shown in Fig. 6(a) to the final depth on YDPM Model MV-1060, 3-axis vertical milling center shown in Fig. 6(b). Workpiece was clamped in a 2-inches precision vice in the first step before laser machining to ensure alignment when shifted to milling center and prevent vibrations during micromilling operation [33]. The BMD Messwell 410 V tool pre-setter shown in Fig. 6(c) is used to obtain precise Z axis measurements.

2.6. Design of experiments

Selecting inappropriate machining parameters can lead to premature tool wear and reduced tool life relative to conventional machining methods. To attain consistent and efficient performance, it is imperative

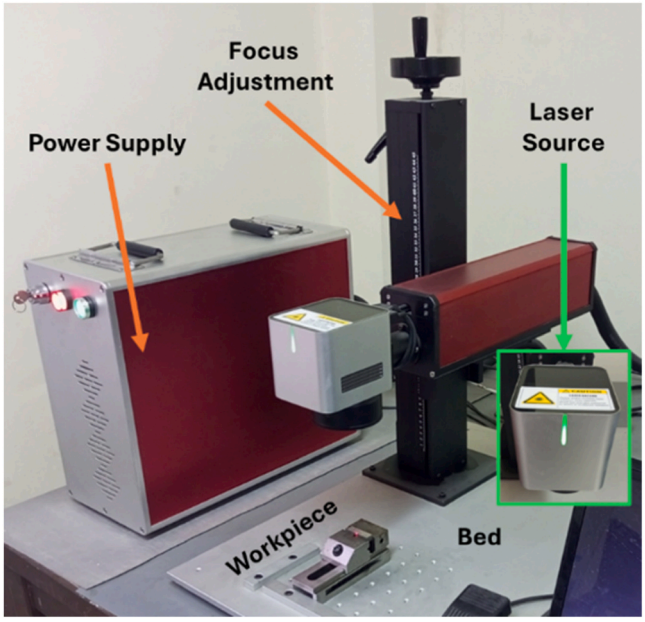

Fig. 4. Laser engraving machine.

Table 5
Details of laser marking machine.

Details	Specifications
Type	TS-20F
Power	20 W
Laser Brand	Maxphotonics (Raycus/IPG Optional
Marking Area	110 mm*100 mm
Marking Depth (max.)	0.5 mm
Marking Speed (max.)	7000 mm/s
Focus Spot Diameter	< 0.01 mm
Output Power of Laser	10–100 % (continuously to be adjusted)

to optimize key milling factors. Optimizing these parameters is fundamental for ensuring machining stability and achieving reliable results [63]. Taguchi method uses orthogonal arrays to optimize factor levels, eliminating the need for full factorial experiments while minimizing the number of trials. By focusing on critical experimental runs, it enhances efficiency in analysis and widely applied to optimize machining, minimizes variations and improves process robustness against environmental and component fluctuations [64]. An experimental layout based on Taguchi L16 orthogonal array was developed, incorporating speed, feed, cutting depth and tool coating type as process variables. Each parameter was evaluated across four levels outlined in Table 6. In contrast to the L-16 orthogonal array which analyzes 4 input parameters at 4 levels each, a full factorial experiment would necessitate 256 experimental

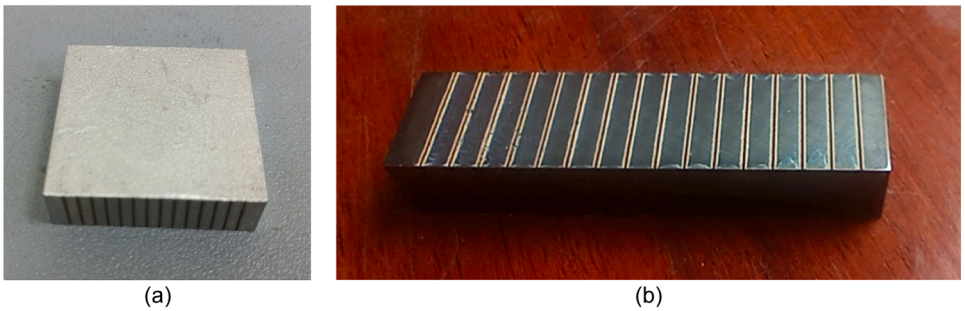

Fig. 3. Inconel 718 (a) Received material form; (b) Prepared workpiece.

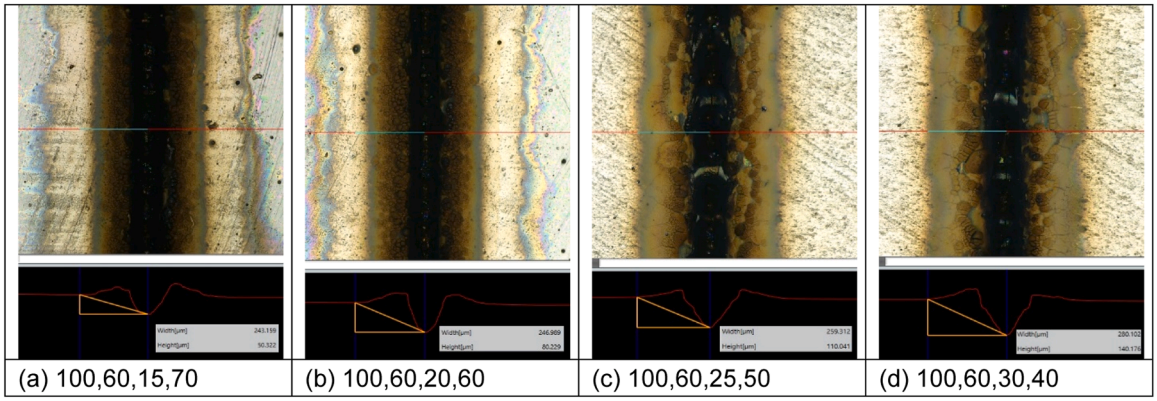

Fig. 5. Laser machined pilot slots for dept: (a) 50 μm; (b) 80 μm; (c) 110 μm; (d) 140 μm with input parameters (Power, Frequency, Loop Count, Speed).

Fig. 6. Experimental setup: (a) Machining operation; (b) vertical milling center; (c) Tool pre-setter.

Table 6
Levels of input variables for micro-milling.

Process parameters	Level 1	Level 2	Level 3	Level 4
Speed (V_c, m/min)	6	7.5	9	10.5
Feed (f_z, μm/tooth)	0.5	1.5	2.5	3.5
Depth of Cut (ap, μm)	60	90	120	150
Tool Coatings	Uncoated	TiAlN	TiSiN	nACo

runs. However, the fractional factorial method of Taguchi reduces this requirement to just 16 experiments. Confirmatory tests were performed to establish the validity of the attained results. The study examined the influence of four distinct machining variables on surface roughness, tool wear and burr formation. These variables included speed tested at four levels, feed rates configured below, and greater than cutting-edge radius, four variations of cutting depth and a selection of both coated and uncoated tools across four categories. Surface roughness, tool wear and burr formation were designated as critical output metrics for assessing machining performance. To quantify the influence of various machining inputs on these response variables, ANOVA was carried out, offering insights into the dominant factors affecting process behavior.

2.7. Measurement of responses

Laser hybrid methodology implemented as a two-stage process to evaluate the final machined slots for key response parameters. Post-processing analysis was carried out using the DSX-1000 Olympus Digital Microscope integrated with software version 1.1.5 as shown in Fig. 7

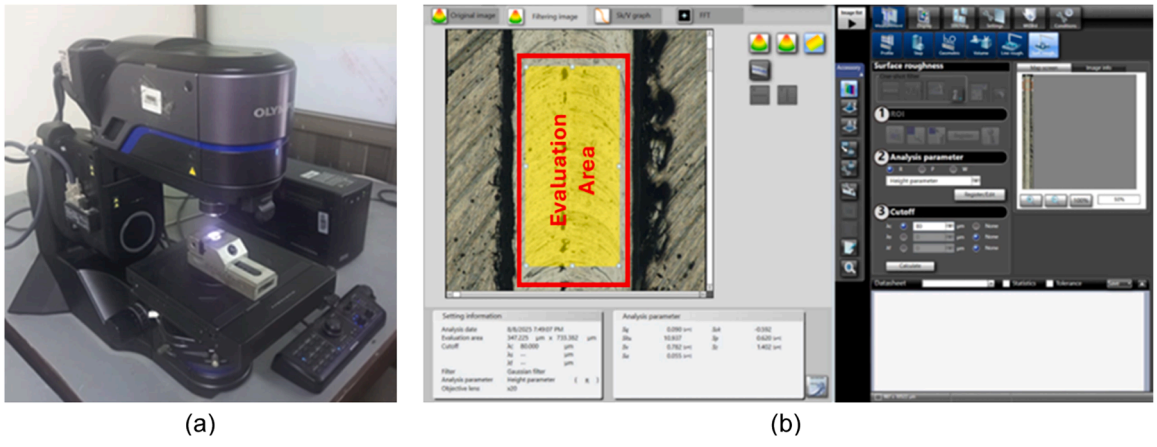

Fig. 7. Measurement setup: (a) Digital microscope; (b) Surface roughness measurement.

(a) and Fig. 7(b). DSX-1000 is a high-precision digital microscope equipped with a telecentric optical system. It features a motorized 10X zoom ratio with automatic calibration, providing a maximum total magnification of up to 9637X. The working distance ranges from 66.1 mm to 0.35 mm, enabling accurate focusing at various height levels. The measurement accuracy in the X–Y plane is ±3 % with a repeatability of 2 %. Illumination is provided by a high-lifetime LED light source (~60,000 h design value). This configuration ensured reliable and repeatable surface and wear characterization in the present study. Critical measurements including surface roughness, tool wear and burr formation were precisely recorded for comprehensive evaluation. This approach reflects current research practices emphasizing high-resolution metrology in advanced micro-machining assessments. Surface roughness was quantified using the areal arithmetic mean height (*Sa*). Areal parameters (*Sa*) provide a more representative measure of micromilled surfaces particularly when ploughing and shearing coexist, because they capture height variations across the measured area rather than along a single profile [65].

3. Results and discussions

Each set of experimental conditions was repeated twice using a fresh cutting tool under consistent settings to minimize the influence of tool wear. The outcomes from these trials are presented in Table 7. Given the precision required in micromachining, even slight disturbances and inaccuracies can significantly influence the results. Differences between the repeated tests were mainly attributed to human error, tool quality variations and inherent machine noise. The experimental data was analyzed using ANOVA [64], with the "lower-the-better" criterion applied to determine the contribution of each factor [33] and evaluate the significance of each factor. Factors yielding p-values below 0.05 were considered significant at a 95 % confidence level [66]. Confirmatory experiments were carried out additionally to validate the ANOVA findings for both best and worst machining scenarios. Effective machining of Inconel 718 demands an in-depth knowledge of its mechanical characteristics, careful selection of cutting tool materials and coatings, as well as precise control over process parameters [12,19,56,57].

3.1. Surface roughness analysis

One of the critical issues encountered in micro-milling is achieving an optimal surface finish because surface roughness directly influences the dimensional accuracy and durability of small-scale components [62]. Traditional machining techniques frequently face limitations in minimizing surface irregularities due to interrupted cutting force phenomenon which is especially prominent in the fabrication of aerospace parts [58]. D. Serje et al. [67] found in their research that primary contributors to surface roughness are tool geometry, machine accuracy, cooling conditions and tool wear.

Surface finish is greatly affected by critical machining parameters including cutting speed, feed rate and depth of cut [12,68]. ANOVA results on surface roughness identifies cutting depth as the most influential factor, accounting for 28.64 % of the overall variability as presented in Table 8. Due to conflicting results, prior research indicates that the effect of depth of cut on surface roughness is still uncertain and difficult to evaluate [69]. In this work, depth of cut has nonlinear behavior but as cutting depth increases, a trend toward increased roughness has been noted shown in Fig. 8. This is often attributed to the generation of excessive heat at deeper cuts which lead to thermal stress

Table 7
L-16 orthogonal array of input parameters with corresponding responses.

Test	Input Parameters				Response Parameters				
	Speed *Vc*	Feed *fz*	DoC *ap*	Tool Coatings	Surface Roughness	Tool Wear		Burr Formation	
						Flank	Face	Width	Height
	(m/min)	(µm/tooth)	(µm)	(t_c)	(µm)	(µm)	(µm)	(µm)	(µm)
1	6	0.5	60	UCoat	0.025	14.63	19.09	201.35	194.37
2	6	1.5	90	TiAlN	0.024	56.29	66.14	75.23	90.41
3	6	2.5	120	TiSiN	0.031	27.85	48.04	231.09	266.09
4	6	3.5	150	nACo	0.038	27.1	59.07	223.18	172.17
5	7.5	0.5	90	TiSiN	0.018	30.89	48.74	228.11	271.26
6	7.5	1.5	60	nACo	0.029	42.39	44.48	257.31	314.17
7	7.5	2.5	150	UCoat	0.022	21.31	45.55	190.23	153.13
8	7.5	3.5	120	TiAlN	0.044	49.43	79.37	70.42	68.17
9	9	0.5	120	nACo	0.031	42.39	82.7	296.03	218.19
10	9	1.5	150	TiSiN	0.026	28.54	73.93	306.27	292.71
11	9	2.5	60	TiAlN	0.013	20.8	32.03	161.43	210.88
12	9	3.5	90	UCoat	0.018	44.85	31.6	158.33	99.11
13	10.5	0.5	150	TiAlN	0.026	43.17	105.14	210.62	77.23
14	10.5	1.5	120	UCoat	0.019	36.91	73.8	150.35	101.21
15	10.5	2.5	90	nACo	0.021	94.52	93.82	129.07	93.83
16	10.5	3.5	60	TiSiN	0.023	60.66	66.84	161.22	146.29
Std Dev					0.008	19.490	23.829	68.061	82.254

Table 8
ANOVA for surface roughness.

Source	DF	Seq SS	Contribution	Adj SS	Adj MS	F-Value	P-Value
Speed (*Vc*)	3	0.000294	15.79 %	0.000294	0.000098	7.01	0.002
Feed (*fz*)	3	0.000427	22.88 %	0.000427	0.000142	10.15	0.000
DoC (*ap*)	3	0.000534	28.64 %	0.000534	0.000178	12.71	0.000
Coatings	3	0.000344	18.43 %	0.000344	0.000115	8.18	0.001
Error	19	0.000266	14.27 %	0.000266	0.000014		
Total	31	0.001866	100.00 %				

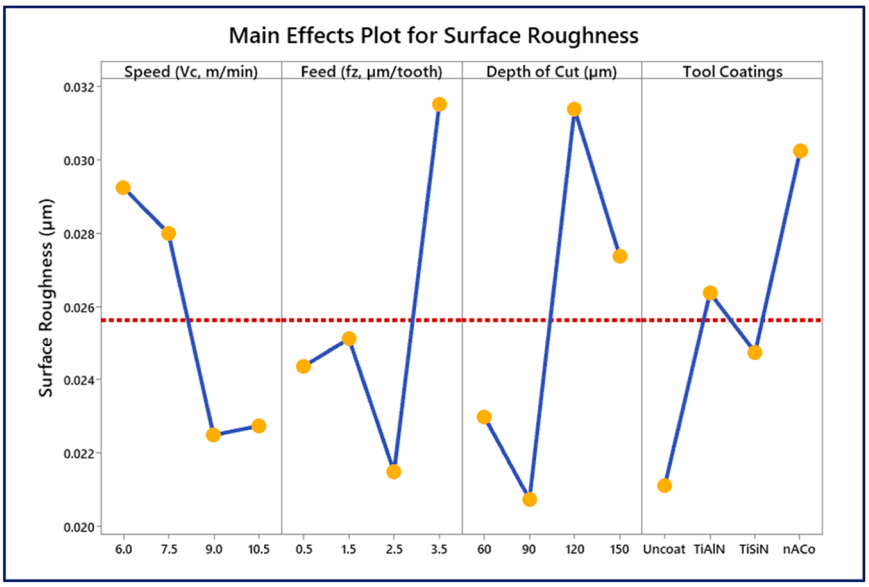

Fig. 8. Surface roughness against machining parameters and tool coatings.

and the formation of microcracks [70]. Zhang and Addona have also concluded that increased depth of cut give rise to cutting forces and chatter at cutting zone ultimately result in higher values of surface roughness [71,72].

Feed rate stands out as the second most influential parameter accounting for 22.88 % of the variation slightly higher than the 18.43 % contribution from tool coating effects. In comparison, cutting speed has a relatively lower impact, contributing 15.79 % to the overall variability. The main effect plots reveal a nonlinear correlation between feed rate and surface roughness as illustrated in Fig. 8. At very low feed rate of 0.5 µm/tooth, the undeformed chip thickness becomes comparable to or smaller than the cutting-edge radius, resulting in a more ploughing-dominated cutting mechanism instead of full chip formation. This size effect minimizes height variations on the machined surface, thereby yielding a smoother finish compared to higher feed values. Surface roughness improves as the feed rate increases initially from 1.5 to 2.5 µm/tooth. However, as the feed rate continues to rise from 2.5 to 3.5 µm/tooth, surface roughness begins to increase again indicating a decline in surface quality at higher feed values. Lu et al. [73] recognized the cutting-edge radius as a critical parameter affecting surface roughness in micromachining operations. Experimental observations reveal a strong correlation between feed rate and the cutting-edge radius indicating that the best surface finish is achieved when the feed rate is set close to the radius of the cutting edge. This relationship is primarily influenced by the interaction between the undeformed chip thickness and the tool edge geometry. Selecting a feed rate significantly below the cutting-edge radius does not yield substantial improvements in surface quality whereas feed rates approximating or slightly exceeding the edge radius result in more effective material removal and smoother surfaces. These findings are consistent with recent research trends emphasizing the influence of tool geometry on micromachining performance. However, employing a lower feed rate in conjunction with a reduced cutting-edge radius leads to a lower residual surface height [67]. U. Maheshwera et al. [74] pointed out that when working with tough materials such as Inconel 718, an increase in feed rate and depth of cut leads to higher surface roughness while elevated cutting speeds tend to produce smoother surfaces [75]. Surface roughness tended to decrease with increasing cutting-speed. A minor increase was observed as the speed rose from 9 to 10.5 m/min. This subtle increase is primarily attributed to thermal dynamics within the cutting zone, as reported by Platt et al. [76].

Analysis of main effect trends for the micromachining process indicates that lowest surface roughness was achieved using uncoated tools. In contrast, tools coated with nACo demonstrated the highest surface roughness while TiSiN coated tools delivered comparatively better results ranking second in performance followed by TiAlN coated tools showing the second highest roughness values. This trend is attributed to the elevated hardness of nACo coated tools which could influence chip formation dynamics [28]. Regardless of the applied machining parameters, numerous studies underscore the critical role of tool wear influencing surface finish during micro-milling. Minimizing tool degradation has been identified as a key strategy for enhancing surface integrity in precision machining applications [77,78].

3.2. *Tool wear analysis*

Tool wear, defined as the loss of tool material due to interactions with the workpiece and chips. It alters cutting forces and is more pronounced in difficult-to-machine materials [79]. Tool wear significantly influences the final quality of micro-machined components due to its direct engagement with the workpiece surface, affecting both dimensional accuracy and surface finish which are key aspects in micromachining. Notably, tool wear is irreversible and negatively impacts these attributes [80]. Khan et al. [81] emphasized that materials with higher temperature strength tend to accelerate tool wear during machining [82].

Gaining insights into the mechanisms of tool wear is essential for enhancing machining efficiency, extending tool life, improving component quality and reducing operational costs [83]. Among the different types of wear, flank wear is considered the most critical due to its direct impact on the stability of the cutting edge and the precision of the machined part. This wear typically develops due to a combination of mechanical pressure, elevated temperatures and chemical reactions during cutting operations. In micro-milling of Inconel 718, the chip–tool contact on the rake face is limited due to the size effect, making crater wear insignificant and flank wear dominant mode of tool degradation [84,85]. While optimizing cutting parameters extend tool life, conventional machining has limitations in minimizing wear [86]. Fig. 9 illustrates the effects of input parameters on tools.

The outcomes of the ANOVA are summarized in Table 9 and Table 10 while Fig. 10 visualizes the main effect plots highlighting the variations in tool flank and face wear with respect to different machining

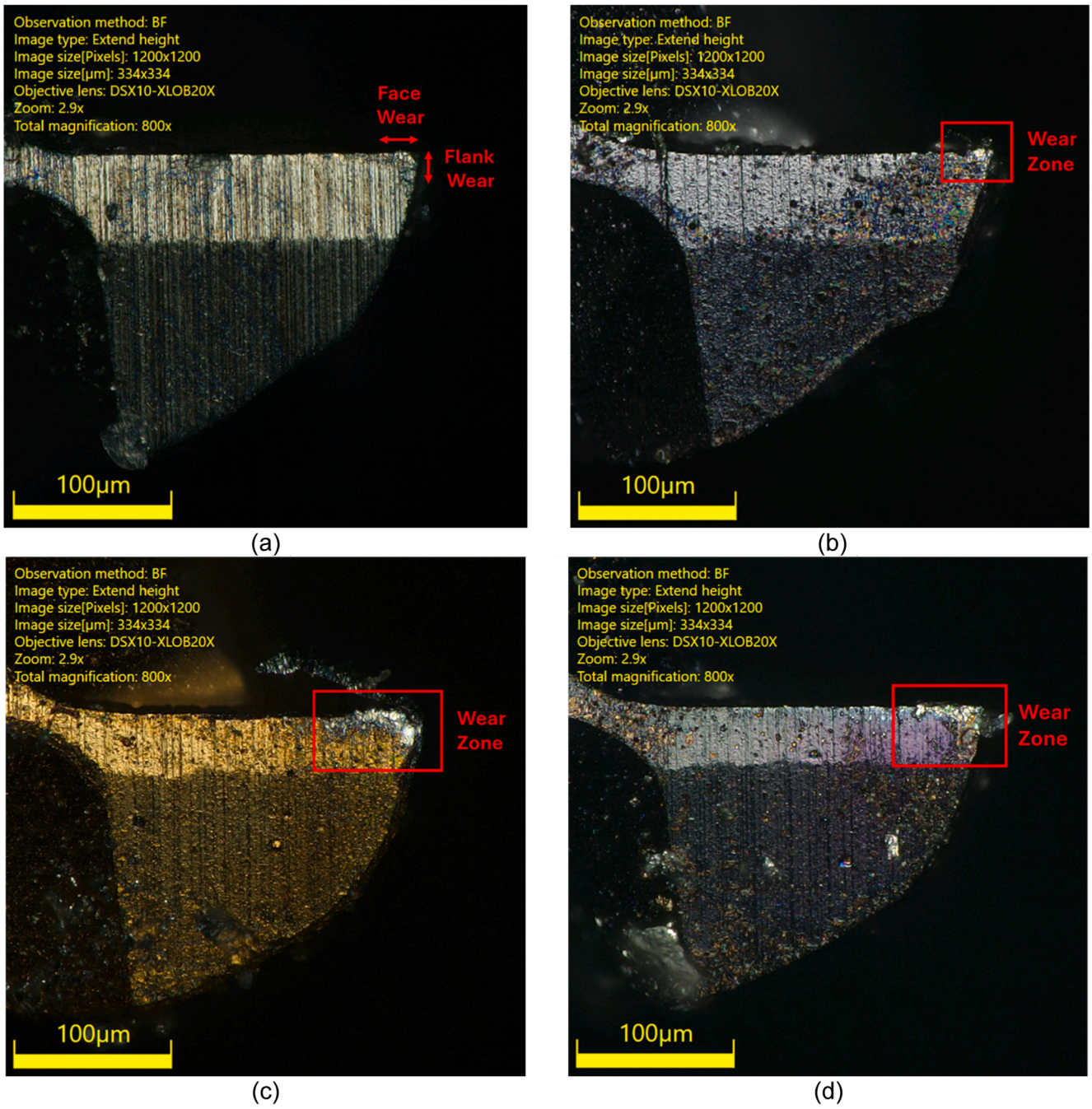

Fig. 9. Tool wear: (a) Uncoated; (b) TiAlN; (c) TiSiN; (d) nACo.

Table 9
ANOVA for tool flank wear.

Source	DF	Seq SS	Contribution	Adj SS	Adj MS	F-Value	P-Value
Speed (*Vc*)	3	3816.0	33.36 %	3816.02	1272.01	15.03	0.000
Feed (*fz*)	3	679.3	5.94 %	679.25	226.42	2.68	0.076
DoC (*ap*)	3	3246.7	28.38 %	3246.69	1082.23	12.79	0.000
Coatings	3	2090.4	18.27 %	2090.42	696.81	8.23	0.001
Error	19	1608.0	14.06 %	1608.02	84.63		
Total	31	11440.4	100.00 %				

parameters. Cutting speed emerges as the most significant contributor to flank wear, accounting for 33.36 % of the variation. This is followed by cutting depth to 28.38 % and tool coating at 18.27 % whereas feed rate shows the least effect with a contribution of just 5.94 %.

In case of face wear, cutting speed and depth of cut again dominate contributing 38.20 % and 28.80 %, respectively, with tool coatings influencing 24.33 % of the variation. These insights reflect the substantial role of cutting dynamics and coating materials in governing tool

Table 10
ANOVA for tool face wear.

Source	DF	Seq SS	Contribution	Adj SS	Adj MS	F-Value	P-Value
Speed (*Vc*)	3	6516.2	38.20 %	6516.22	2172.07	41.96	0.000
Feed (*fz*)	3	494.0	2.90 %	494.00	164.67	3.18	0.048
DoC (*ap*)	3	4912.9	28.80 %	4912.91	1637.64	31.63	0.000
Coatings	3	4150.4	24.33 %	4150.43	1383.48	26.72	0.000
Error	19	983.6	5.77 %	983.62	51.77		
Total	31	17057.2	100.00 %				

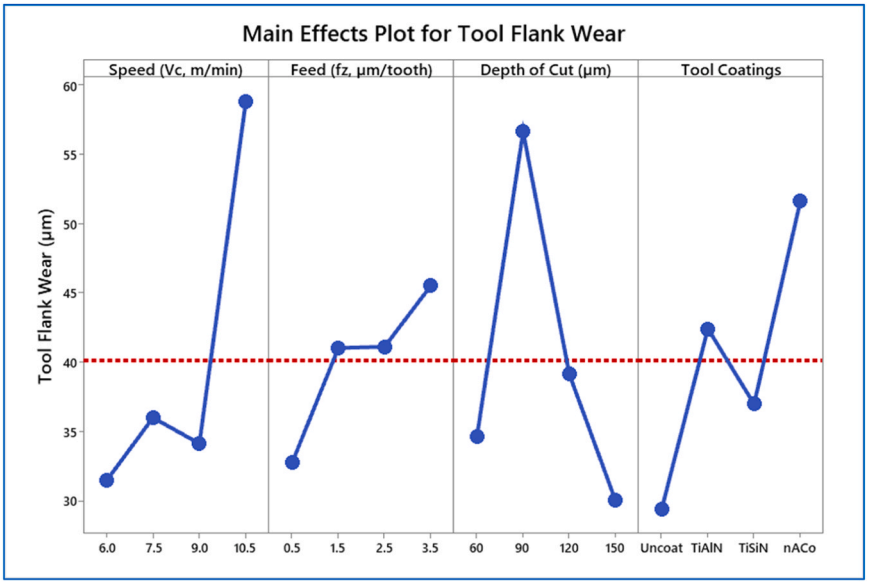

(a)

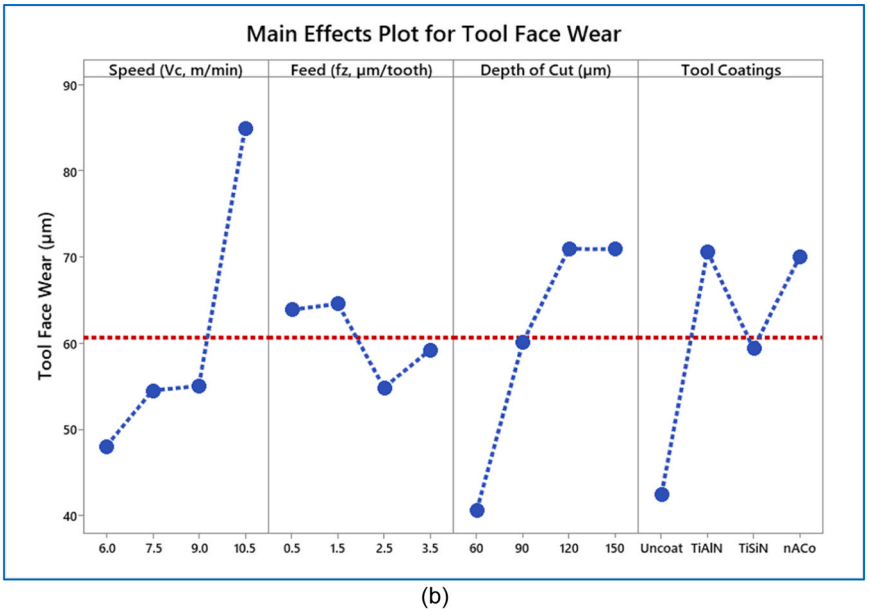

(b)

Fig. 10. Main effect plot of tool wear: (a) Flank wear; (b) Face wear.

wear behavior during precision micromachining.

Fig. 11 illustrates the response behavior corresponding to each individual input parameter. An increase in cutting speed leads to a noticeable rise in both flank and face wear. This is primarily attributed to elevated thermal loads in the cutting zone which led to the softening of the tool material and intensifying chemical interactions with the workpiece. These conditions promote wear mechanisms such as adhesion and diffusion, accelerating tool degradation [87,88]. M. Abdul Hadi et al. [89] also highlighted that poor thermal conductivity of Inconel 718 traps heat at the tool–chip interface, promoting notch wear on the flank due to dominant adhesion and abrasion mechanisms. An increase in feed rate leads to greater tool wear primarily due to the increase in shear plane area and undeformed chip thickness. These changes result in higher material removal rates and elevated normal forces acting on the tool. This relationship has been widely recognized in several investigations including the findings of Cui et al. [90]. Fig. 11 illustrates

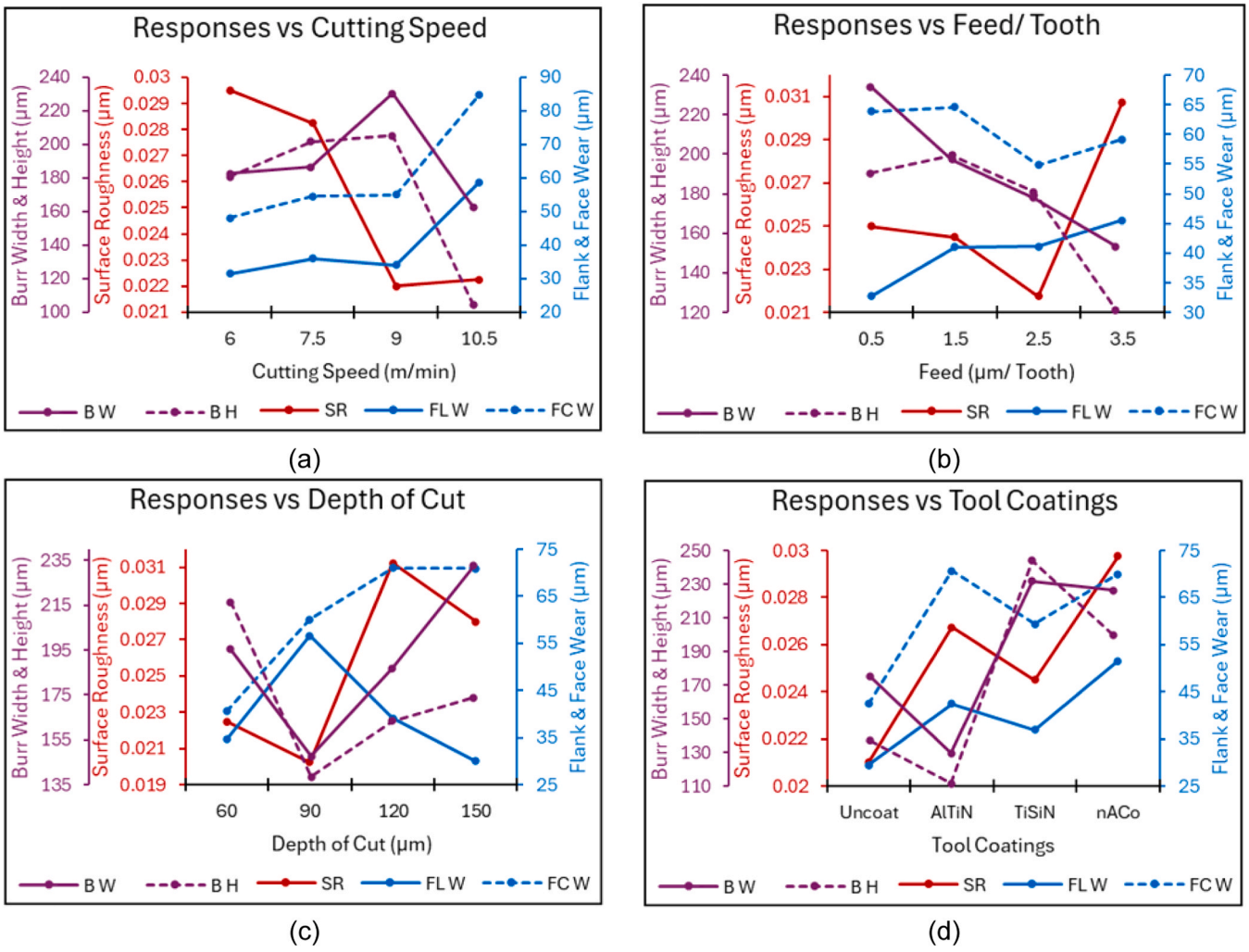

Fig. 11. Main effect plots for responses against: (a) Cutting speed; (b) Feed; (c) Depth of cut; (d) Tool coatings.

the nonlinear trend of face wear as feed rate changes from 0.5 to 3.5 µm/tooth with a noticeable effect at 2.5 µm/tooth, approximately equal to the cutting-edge radius of tool. Higher feed rates reduce tool-workpiece engagement leading to lower both thermal and mechanical stresses thereby minimizing tool wear. N. Anand Krishnan and J. Mathew demonstrated that when the feed rate is below the cutting-edge radius, plowing dominates the material removal whereas feed rates above the radius shift the mechanism to shearing [85].

The depth of cut significantly influences the machining dynamics of Inconel 718, affecting cutting force intensity, heat generation, tool wear progression and material removal rate. Increasing the depth of cutting elevates the mechanical load and accelerates tool wear but also enhances productivity through higher material removal. Conversely, reducing the depth compromises machining efficiency [91,92]. Optimization of cutting depth is vital to maintain a balance between the alloy's mechanical properties, cutting tool limitations and desired process outcomes [12,91–93]. Additionally, refined depth of cut selection contributes to better chip segmentation, reduced cutting resistance and more efficient material removal when machining high-strength Inconel 718 [57,94].

Fig. 11 indicates that a higher depth of cut reduces flank wear but increases face wear, due to varying mechanical and thermal effects on different tool regions. This contrast arises from the different mechanical and thermal stresses acting on specific tool areas, which are particularly impactful at the micro-scale. At lower depths, material removal is primarily driven by ploughing and surface rubbing instead of shearing. Aramcharoen and Mativenga [45] found that increasing the depth of cut in micro-milling lowers specific cutting forces, reducing overall wear due to limited tool–material interaction which minimizes abrasive and adhesive wear [45]. Jin et al. [95] highlighted that greater depths of cut, associated with higher material removal rates help dissipate heat more effectively, thereby lessening thermally induced tool wear. However, deeper cuts also increase tool–chip contact, raising friction and leading to higher face wear, primarily from adhesive mechanisms as chips slide across the tool surface.

Fig. 11(d) shows that uncoated tools experience the least face and flank wear compared to coated ones. Among coated variants, TiSiN provided better wear resistance, while TiAlN and nACo coatings exhibited higher and nearly similar wear rates. The superior performance of uncoated carbide tools is attributed to their sharp edges and smoother surfaces, as coatings often introduce surface flaws that degrade performance. Failures such as chipping, cracking, and delamination indicate poor coating adhesion, underlining the importance of optimizing interlayer bonding [96–99]. Moreover, high temperatures during machining can lead to thermal softening and coating separation due to excessive heat and material buildup on coated tools [100,101].

Table 11
ANOVA for Burr Width.

Source	DF	Seq SS	Contribution	Adj SS	Adj MS	F-Value	P-Value
Speed (*Vc*)	3	19553	14.06 %	19552.7	6517.6	17.96	0.000
Feed (*fz*)	3	27863	20.04 %	27862.5	9287.5	25.59	0.000
DoC (*ap*)	3	29113	20.94 %	29112.8	9704.3	26.74	0.000
Coatings	3	55617	40.00 %	55617.0	18539.0	51.09	0.000
Error	19	6895	4.96 %	6894.7	362.9		
Total	31	139040	100.00 %				

Table 12
ANOVA for Burr Height.

Source	DF	Seq SS	Contribution	Adj SS	Adj MS	F-Value	P-Value
Speed (*Vc*)	3	52754	25.98 %	52754.1	17584.7	38.70	0.000
Feed (*fz*)	3	29836	14.69 %	29836.2	9945.4	21.89	0.000
DoC (*ap*)	3	25266	12.44 %	25265.6	8421.9	18.53	0.000
Coatings	3	86566	42.63 %	86565.9	28855.3	63.50	0.000
Error	19	8634	4.25 %	8633.8	454.4		
Total	31	203056	100.00 %				

3.3. Burr formation analysis

In micro-milling operations, Inconel 718 exhibits a strong tendency to generate substantial burrs, primarily due to its inherent plastic deformation behavior, high adhesion to cutting tools and poor chip breakability. The extent and nature of burr generation are strongly influenced by a combination of machining parameters, tool geometry and the intrinsic mechanical and thermal properties of the material [102,103]. In up milling, when cutting thickness is below the minimum, only elastic deformation occurs without chip formation. As thickness increases beyond this threshold, chips form and plastic shear deformation dominates. In down milling, when reduced below a certain value, chips either break or remain in the groove, forming burrs through extrusion (up milling) or incomplete fracture (down milling) [102]. Burr formation adversely impacts product dimensional accuracy and often demands additional deburring processes, which can be both costly and technically intricate. This challenge is particularly critical in the context of micro-scale components, where small geometry increases vulnerability to mechanical damage during post-processing. Improper deburring techniques can introduce residual stresses, potentially compromising structural integrity and functional performance [77].

Burrs are observed to form more extensively on the down-milling side than on the up-milling side, exhibiting greater burr width and height. This phenomenon is attributed to the relatively lower cutting-edge velocity encountered during down milling, whereas the up-milling side experiences higher edge speeds which contributes to reduced burr development. Previous investigations on micro-milling have consistently reported this directional dependency in burr behavior [48]. To accurately assess the most critical case, evaluation focused exclusively on burrs formed during down milling by quantifying the maximum burr width and height recorded in each experimental trial.

Table 11 and Table 12 present the ANOVA outcomes while Fig. 11 illustrates the response trends relative to each individual machining parameter. Fig. 12 illustrates the main effect plots across all considered variables. Among the influencing factors, tool coatings emerged as the most dominant, accounting for 40 % and 42.63 % of the variance in burr width and burr height, respectively. TiAlN-coated and uncoated tools yielded the most favorable results in terms of reduced burr formation. TiAlN-coated tools exhibited reduced burr width and height, which can be attributed to the coating's high thermal stability and its ability to form protective Al_2O_3 films during cutting. These oxide layers improve chip flow, stabilize the chip–tool contact, and minimize adhesive interactions with Inconel 718. Consequently, wear progression is reduced, and the cutting edge geometry is better preserved, promoting cleaner shearing and smaller burr formation [98]. In contrast, TiSiN and nACo-coated tools were associated with significantly higher burr dimensions. The TiSiN-coated tool had higher coefficient of friction, which elevated cutting temperatures and intensified material deformation, ultimately leading to increased burr formation [28,104,105].

Feed contributes 20.04 % and 14.69 % against burr width and height, respectively. The value of burrs was higher at first, then dropped and produced lower values at higher feed levels. Burr width decreases as feed per tooth increases, reaching its lowest value at 3.5 μm/tooth due to a shift in the dominant material removal mechanism. At higher feed rates, cutting transitions from ploughing to shearing, allowing the tool edges to engage more effectively and remove material cleanly with minimal plastic deformation reducing burr size. Lower feed rates, on the other hand promote ploughing in which material is displaced instead of being sheared, causing to undergo plastic deformation and generate larger burrs due to inefficient cutting action [104,106,107].

Contribution of cutting speed was noted 14.06 % and 25.98 % for burr width and height, respectively. An increase in cutting speed generally leads to a reduction in burr width and height, as indicated by the downward trend in the main effect plots. This trend is associated with a decrease in cutting forces and reduced tool-chip contact time, which lowers heat transfer to the chip and increases heat transfer to the tool tip. Although higher speeds elevate shear zone temperatures, the friction at the tool-chip interface reduces, diminishing chip adhesion and heat buildup, thereby limiting burr formation [108–111]. Additionally, the uncut chip thickness declines with increased speed, contributing further to reduced burr size especially in hard-to-machine alloys [87,104]. Least contribution of 12.44 % was observed in burr height for depth of cut and it was 20.94 % for burr width. As the depth of cut increases, the uncut chip thickness also grows, which leads to a corresponding increase in both burr width and burr length [104].

3.4. Optimization of individual process responses

Single-objective optimization focuses on optimizing a specific response by adopting the smaller is better approach without considering conflicting trade-offs with other responses. Main effect plots revealed that the optimal response varies across different input parameter settings. To validate the statistical reliability and authenticity of the experimental design, separate confirmatory experiments were repeated three times using the most and least effective sets of identified parameters. The outcomes of these tests, along with the corresponding input

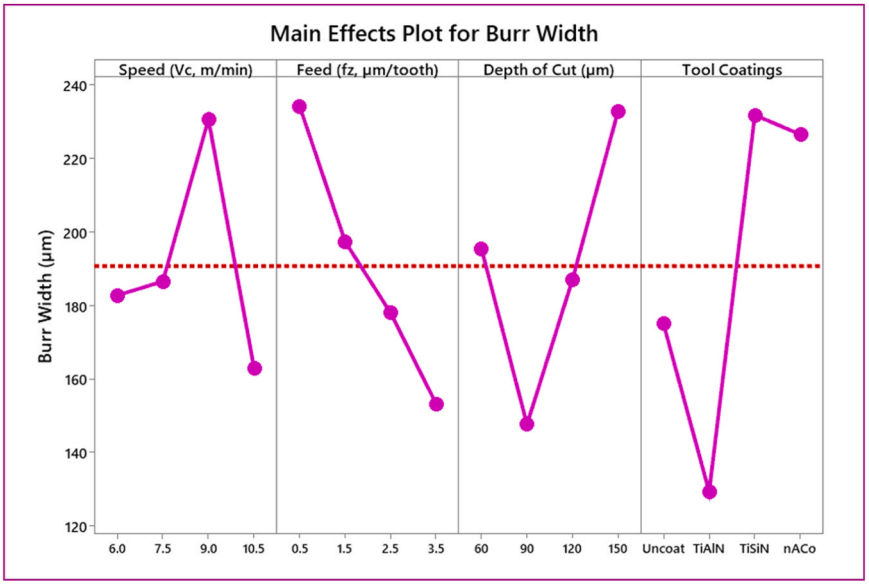

(a)

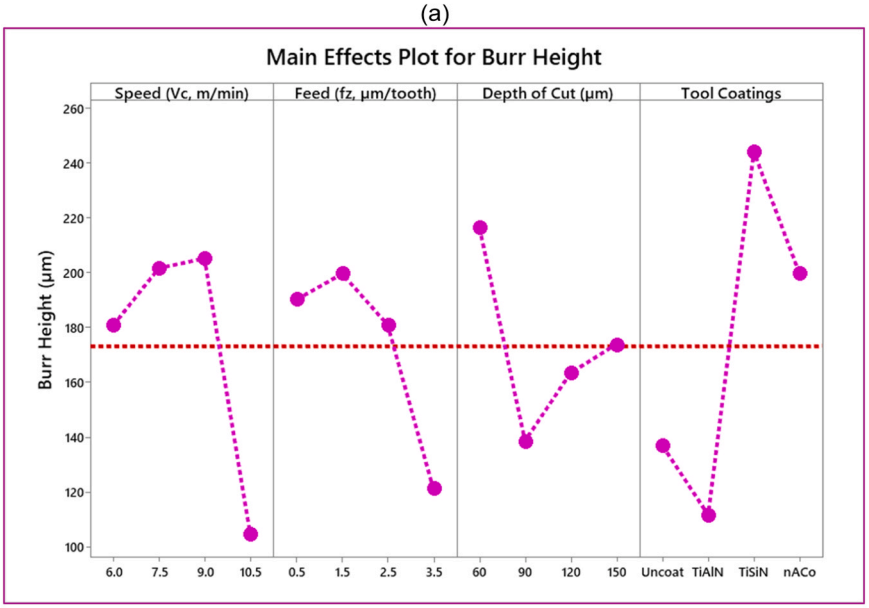

(b)

Fig. 12. Main effect plots of (a) Burr Width; (b) Burr Height.

Table 13
Optimal combination of input parameters for individual response.

	Response Parameters									
		Best				Worst				
	Surface Roughness	Tool Wear		Burr Formation		Surface Roughness	Tool Wear		Burr Formation	
	Ra (µm)	Flank (µm)	Face (µm)	Width (µm)	Height (µm)	Ra (µm)	Flank (µm)	Face (µm)	Width (µm)	Height (µm)
Output Result	0.012	14.06	17.98	68.92	64.83	0.047	98.21	111.22	309.61	297.21
Speed (V_c, m/min)	9	6	6	10.5	10.5	6	10.5	10.5	9	9
Feed (f_z, µm/tooth)	2.5	0.5	2.5	3.5	3.5	3.5	3.5	1.5	0.5	1.5
Depth of Cut (µm)	90	150	60	90	90	120	90	120	150	60
Tool Coatings	Uncoat	Uncoat	Uncoat	TiAlN	TiAlN	nACo	nACo	TiAlN	TiSiN	TiSiN

parameters, are presented in Table 13. The analysis reveals that each output response requires a distinct set of optimal input conditions. Enhancing one performance metric may adversely affect others, emphasizing the importance of reaching a trade-off that meets all performance requirements. This trade-off underscores the need for multi-objective optimization, which balances conflicting objectives to provide a more comprehensive and effective solution for complex machining problems [112–116].

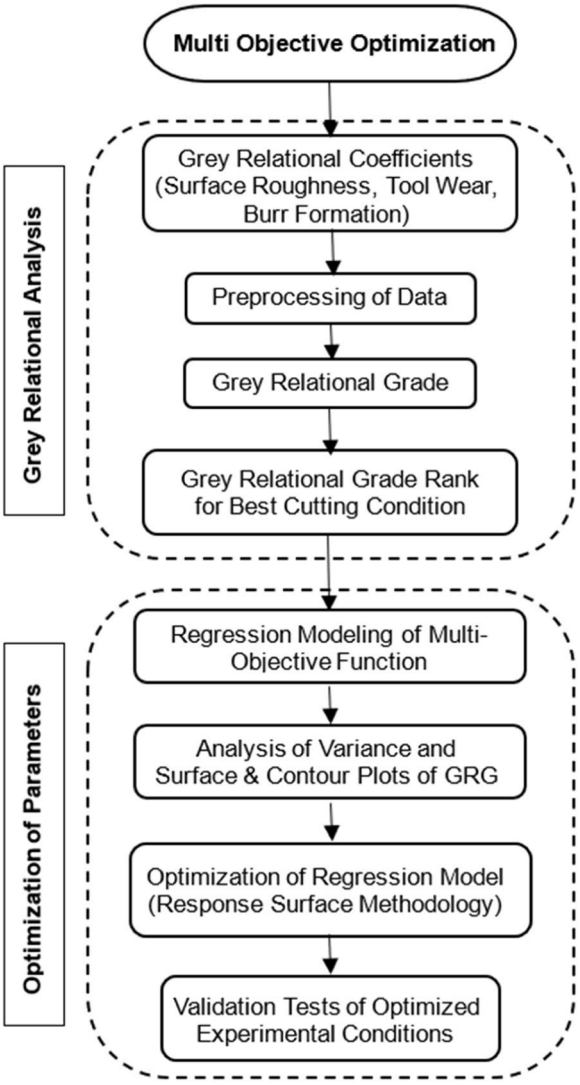

Fig. 13. Scheme for multi objective optimization.

4. Multi-objective optimization

Multi-Objective Optimization (MOO) is a crucial decision-making technique used when multiple conflicting objectives must be optimized simultaneously and to identify the best alternative among multiple competing options where traditional single-objective optimization methods fail to provide satisfactory solutions. ANOVA based optimization of individual output responses under various input parametric conditions is revealed by Table 13 analysis, based on main effect plots displayed in Fig. 10 and Fig. 12.

GRA derived from Grey System Theory, is a powerful technique, offers an effective solution strategy to solve such complex problems. GRA is particularly useful when dealing with limited data, incomplete information or uncertain environments, making it suitable for engineering, manufacturing and industrial applications where trade-offs must be made between different criteria. The scheme for multi-objective optimization is elaborated in Fig. 13. A multi-response problem is reduced to a single distinctive function using GRA, based on the Taguchi approach. The formulation of Grey Relational Analysis (GRA) follows the standard definitions of Grey System Theory and has been widely implemented in several Taguchi–GRA-based studies on machining and multi-response optimization [81,117–121].

4.1. Pre-processing of data

Data preprocessing is a crucial step in maintaining uniformity and facilitating meaningful comparisons, particularly in decision matrices which involve numerous alternatives assessed against multiple criteria. Each alternative is assessed across several parameters with varying units and scales leading to skewed outcomes. To mitigate this, normalization is carried out using Eq. (1) for surface roughness, tool wear, and burr formation on a comparable scale between 0 and 1, with the idea that lower values indicate better performance.

$$X_{ij}^{*} = \frac{\max(X_{ij}) - X_{ij}}{\max(X_{ij}) - \min(X_{ij})} \tag{1}$$

The variables X_{ij} and X_{ij}^{*} refer to the actual and normalized values, respectively while $\max(X_{ij})$ and $\min(X_{ij})$ indicate the highest and lowest measurements for each response.

4.2. Grey relational coefficient (GRC)

After normalizing data, the Grey Relational Coefficient (GRC) is computed for each alternative to evaluate its proximity to the ideal solution. The reference sequence X_0^{*} is derived by selecting the best normalized value for every criterion. Eq. (2) is then used to calculate the deviation sequence Δ_{ij}, representing the gap between the normalized values and the reference sequence.

$$\Delta_{ij} = \left| X_0^{*} - X_{ij}^{*} \right| \tag{2}$$

X_0^{*} represent the reference value (ideal solution, usually the best value for each criterion) while X_{ij}^{*} indicate the normalized value of the alternative *i* for criterion j. The GRC for each alternative *i* with respect to each criterion *j* is determined in accordance with Eq. (3).

$$GRC_{ij} = \frac{\Delta_{\min} + \xi\Delta_{\max}}{\Delta_{ij} + \xi\Delta_{\max}} \tag{3}$$

$\Delta_{\min}$ and $\Delta_{\max}$ represent the smallest and largest deviation values observed among all criteria and alternatives. The distinguishing coefficient, denoted as ξ, is generally assigned a value of 0.5 when equal importance is assumed for all parameters to regulate the sensitivity of the evaluation. GRC values lie within the range of 0–1, where values approaching 1 signify a stronger link with the reference sequence.

4.3. Grey Relational Grade (GRG)

The Grey Relational Grade (GRG) serves as a measure of the overall effectiveness or ranking of each alternative. This is achieved by combining the GRCs through a weighted approach. When all criteria are considered equally important, a simple mean is applied. The GRG corresponding to each alternative *i* is computed as shown in Eq. (4).

$$GRG_i = \sum_{j=1}^{m} \omega_j \quad .GRC_{ij} \tag{4}$$

ω_j is the weight assigned to criterion j (sum of all weights equals 1) while m is the total number of criteria.

4.4. GRG rank

The alternatives were ordered according to their GRG scores. A higher GRG value reflects a stronger alignment with the ideal outcome whereas a lower value signifies a weaker association. In the decision-making process, the option with the highest ranking is regarded as the best option. Table 14 shows the experimental runs and associated GRG values. Among all trials, the highest GRG was observed in Test No. 11, which involved a TiAlN-coated tool operating at a cutting speed of 9 m/min, a feed rate of 2.5 μm/tooth and a depth of cut of 60 μm.

Table 14
GRCs and GRG with ranking against input machining conditions.

Test	Input Parameters				Grey Relational Coefficient (GRC)					Grey Relational Grade (GRG)	Rank
	Speed *Vc*	Feed *fz*	DoC *ap*	Tool Coatings	Surface Rough-ness	Tool Wear		Burr Formation			
						Flank	Face	Width	Height		
	(m/min)	(μm/tooth)	(μm)	(t_c)	Ra (μm)	(μm)	(μm)	(μm)	(μm)		
1	6	0.5	60	UCoat	0.387	0.000	0.000	0.555	0.513	0.706217	2
2	6	1.5	90	TiAlN	0.355	0.521	0.547	0.020	0.090	0.671948	4
3	6	2.5	120	TiSiN	0.581	0.165	0.336	0.681	0.805	0.523672	13
4	6	3.5	150	nACo	0.806	0.156	0.465	0.648	0.423	0.528131	12
5	7.5	0.5	90	TiSiN	0.161	0.204	0.345	0.669	0.826	0.572775	8
6	7.5	1.5	60	nACo	0.516	0.347	0.295	0.792	1.000	0.486228	14
7	7.5	2.5	150	UCoat	0.290	0.084	0.307	0.508	0.345	0.639215	6
8	7.5	3.5	120	TiAlN	1.000	0.436	0.701	0.000	0.000	0.656847	5
9	9	0.5	120	nACo	0.581	0.347	0.739	0.957	0.610	0.449987	16
10	9	1.5	150	TiSiN	0.419	0.174	0.637	1.000	0.913	0.482492	15
11	9	2.5	60	TiAlN	0.000	0.077	0.150	0.386	0.580	0.732462	1
12	9	3.5	90	UCoat	0.161	0.378	0.145	0.373	0.126	0.694412	3
13	10.5	0.5	150	TiAlN	0.419	0.357	1.000	0.594	0.037	0.569741	10
14	10.5	1.5	120	UCoat	0.194	0.279	0.636	0.339	0.134	0.637475	7
15	10.5	2.5	90	nACo	0.258	1.000	0.868	0.249	0.104	0.570705	9
16	10.5	3.5	60	TiSiN	0.323	0.576	0.555	0.385	0.318	0.544596	11

5. Response surface methodology (RSM)

RSM is an advanced statistical tool used to optimize processes that are affected by several interacting variables. It supports the systematic improvement of experimental outcomes through mathematical modeling and statistical techniques. RSM combines data-fitting techniques, statistical analysis and experimental design to optimize processes more precisely and efficiently than the Taguchi Method.

5.1. Regression analysis

Regression analysis is a statistical approach used to identify the relationship between several input factors and their corresponding response variables. This technique is valuable in multi-objective optimization, where trade-offs between conflicting goals must be effectively managed to attain the optimal result. The optimization process encompassed the development of a regression model for the multi-objective function, verification of the model through ANOVA and refinement of results using RSM.

5.2. Regression modeling of multi-objective function

A predictive mathematical model was formulated using experimental data through Minitab software to express the GRG as a function of key input variables like cutting speed, feed rate, depth of cut, and tool coating type. In this study, machining parameters such as cutting speed, feed, and depth of cut were treated as continuous variables while tool coatings were handled as categorical variables. The regression equations derived through RSM are provided from Eq. (5) to Eq. (8). These models were subsequently optimized using RSM techniques to identify the optimal settings for enhanced GRG performance.

$$GRG(V_c, f_z, ap, Uncoat) = 0.570 + 0.0272V_c - 0.141f_z + 0.00205ap + 0.00106V_c^*V_c - 0.0013f_z^*f_z - 0.000006ap^*ap + 0.0050V_c^*f_z - 0.000403V_c^*ap + 0.000983f_z^*ap \quad (5)$$

$$GRG(V_c, f_z, ap, TiAlN) = 0.595 + 0.0272V_c - 0.141f_z + 0.00205ap + 0.00106V_c^*V_c - 0.0013f_z^*f_z - 0.000006ap^*ap + 0.0050V_c^*f_z - 0.000403V_c^*ap + 0.000983f_z^*ap \quad (6)$$

$$GRG(V_c, f_z, ap, Uncoat) = 0.443 + 0.0272V_c - 0.141f_z + 0.00205ap + 0.00106V_c^*V_c - 0.0013f_z^*f_z - 0.000006ap^*ap + 0.0050V_c^*f_z - 0.000403V_c^*ap + 0.000983f_z^*ap \quad (7)$$

$$GRG(V_c, f_z, ap, Uncoat) = 0.399 + 0.0272V_c - 0.141f_z + 0.00205ap + 0.00106V_c^*V_c - 0.0013f_z^*f_z - 0.000006ap^*ap + 0.0050V_c^*f_z - 0.000403V_c^*ap + 0.000983f_z^*ap \quad (8)$$

Contour plots are valuable tools for examining how two input variables jointly affect a response outcome. Fig. 14 illustrate the contour graphs for the four different cutting tools, highlighting the effect of varying input parameters on the GRG. These visualizations provide a clear depiction of how variations in input settings impact GRG performance. The results indicate that maximum GRG values are typically observed when both the cutting speed and feed rate are set at lower ranges.

5.3. Analysis of variance for model validation

ANOVA was conducted on GRG values to assess the significance of each parameter and evaluate the correctness of the constructed regression models. The summarized findings in Table 15 reveal that among all factors, tool coating is the most dominant factor influencing the GRG by contributing 73.68 % of the total. The subsequent influential factor identified is depth of cut, contributing 10.80 % whereas the effects of cutting speed and feed were comparatively minimal.

5.4. Regression model optimization

RSM was used to optimize the regression model created in Eq. (6) through Equation (9) after its validation to obtain the best machining conditions. RSM is a statistical and mathematical framework employed for optimizing processes influenced by several variables. The response surface optimizer revealed the ideal parameter settings with a 95 % confidence level that led to the highest GRG value, achieving minimal surface roughness, reduced tool wear and lower burr formation. Fig. 15 illustrates the machining parameters for the optimized results, which include a cutting speed of 10.5 m/min, feed rate of 2.6 μm/tooth, depth of cut of 60 μm and use of uncoated tool. To confirm the validity of these results, additional experimental runs were conducted.

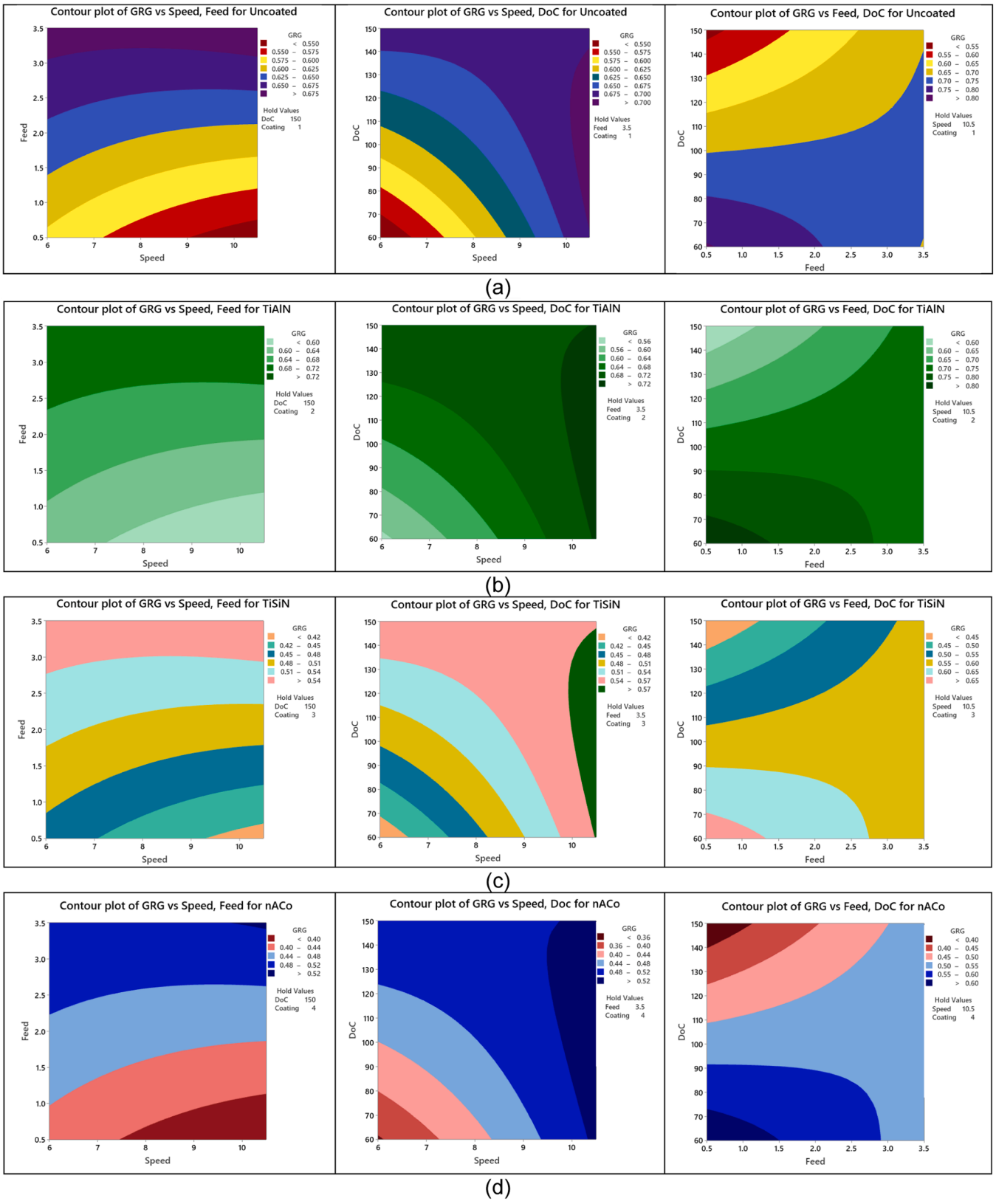

Fig. 14. Contour plots of GRG vs machining conditions for tools: (a)uncoated; (b)TiAlN; (c)TiSiN; (d)nACo.

Table 15
ANOVA for developed regression model.

Source	DF	Seq SS	Contribution	Adj SS	Adj MS	F-Value	P-Value
Model	8	0.108992	95.76 %	0.108992	0.013624	19.77	0.000
Linear	5	0.100128	87.97 %	0.102549	0.020510	29.76	0.000
Feed	1	0.003972	3.49 %	0.003972	0.003972	5.76	0.047
DoC	1	0.012292	10.80 %	0.014713	0.014713	21.35	0.002
Coatings	3	0.083864	73.68 %	0.083864	0.027955	40.56	0.000
Feed*Coatings	3	0.008864	7.79 %	0.008864	0.002955	4.29	0.052
Error	7	0.004825	4.24 %	0.004825	0.000689		
Total	15	0.113817	100.00 %				

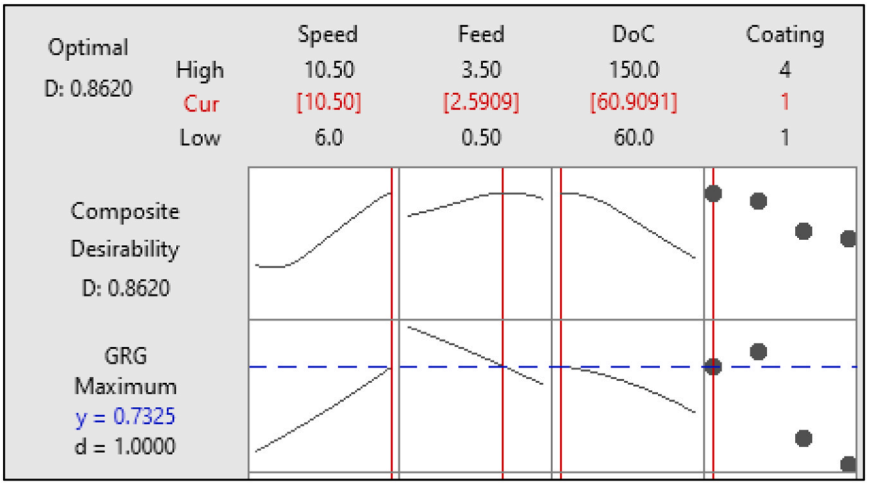

Fig. 15. Response surface optimization against GRG for input conditions. * 1 = uncoated tool.

Table 16
Comparison of responses for optimized best initial experimental run.

Test	Input Parameters				Response Parameters				
	Speed *Vc*	Feed *fz*	DoC *ap*	Coatings	Surface Rough-ness	Tool Wear		Burr Formation	
	(m/min)	(µm/tooth)	(µm)	(t_c)	Ra (µm)	Flank (µm)	Face (µm)	Width (µm)	Height (µm)
Best Run	9	2.5	60	TiAlN	0.013	20.8	32.03	161.43	210.88
Optimized Run	10.5	2.6	60	Uncoated	0.010	16.23	23.67	126.31	157.07

5.5. Validation experiments

The performance of the optimized machining parametes was assessed by comparison with the outcomes of the highest-performing trial Test No. 11 as presented in Table 16. The optimized conditions yielded significant improvements across all output measures. Surface roughness showed the highest reduction at 23.08 %. Tool flank and face wear were reduced by 21.97 % and 26.1 %, while burr width and height reduced by 21.76 % and 25.52 %, respectively, indicating a substantial boost in overall machining performance.

6. Conclusions

This study executed a targeted experimental approach to fill the prevailing research void by evaluating an optimized matrix of machining parameters integrated with multiple tool coating options for laser hybrid micro-milling of Inconel 718. Challenges such as the high sensitivity of micromachining to minor disturbances, variations due to human error, inherent machine noise, and maintaining alignment accuracy during the transfer of the workpiece from the laser setup to the CNC milling machine were addressed through careful calibration, use of a precision vice, and maintenance of controlled operating conditions. Statistical tools including ANOVA and GRA were employed to systematically interpret the experimental data and quantify the influence of each machining input variable on critical performance indicators such as surface roughness, tool wear and burr formation. The outcomes of this investigation provide significant knowledge advancement by revealing the complex synergistic relationships between machining parameters, coating characteristics and their consequential effects on surface quality, tool lifespan and burr mitigation. These findings highlight the vital role of selecting appropriate coatings and accurately adjusting process parameters to achieve optimal machining performance.

1. The desired depths of laser generated pilot slots were achieved through the strategic modulation of key processing parameters including laser power, scanning speed, loop repetition and operational frequency. Elevated levels of frequency and laser power facilitated the stable and uniform formation of slots which significantly mitigated the formation of recast layers and minimized particulate debris within the machined zones.
2. The analysis revealed that surface roughness is governed by a combination of machining variables, with cutting speed, feed per tooth, depth of cut and tool coating contributing 15.79 %, 22.88 %, 28.64 % and 18.43 %, respectively. Uncoated tools demonstrated

superior performance by producing the lowest surface roughness whereas nACo coatings exhibited comparatively higher roughness values. A nonlinear dependency was identified between surface roughness and feed rate while increasing cutting speed led to smoother surfaces. This behavior is predominantly primarily attributed to the thermal softening phenomena occurring in the machining zone.

3. Flank and face wear were primarily governed by variations in cutting speed and depth with contributions of 33.36 % and 28.38 % for flank wear, and 38.20 % and 28.80 % for face wear, respectively. Flank wear exhibited a general increase with all process variables except depth of cut. Face wear, conversely, demonstrated an increasing trend with cutting speed and depth of cut while showing a non-linear trend, initially decreasing and then increasing with higher feed rates. Uncoated tools performed comparatively better wear resistance while tools with nACo coating experienced the most severe wear degradation.
4. Tool coating emerged to be the leading feature in determining burr formation contributing 40 % to burr width and 42.63 % to burr height, respectively. Depth of cut and cutting speed comes next with contribution of 20.94 % for burr width and 25.98 % for burr height, respectively. Burr width exhibited a decreasing trend with elevated cutting speed and feed, while it raised with greater depth of cut. A comparable trend was identified for burr height, which decreased with increased feed and cutting speed but rose with higher cutting depths. Among the tool coatings assessed, TiAlN yielded the lowest burr width and height whereas nACo-coated tools consistently produced the highest burr dimensions in both categories.
5. GRA revealed that the most favorable machining conditions were achieved using TiAlN-coated tools under a cutting speed of 9 m/min, feed per tooth of 2.5 μm and a depth of cut of 60 μm. In contrast, the least favorable conditions were associated with nACo-coated tools at feed rate of 0.5 μm per tooth, depth of cut of 120 μm and same cutting speed of 9 m/min. Additionally, ANOVA performed on the regression model derived from Grey Relational Grades identified tool coating type as the most dominant factor contributing 73.68 % to performance variation followed by cutting depth at 10.80 %.
6. Response Surface Methodology established the optimal machining conditions for uncoated tools with parameter values set at 10.5 m/min speed, 2.6 μm/tooth feed and 60 μm depth of cut. Subsequent validation experiments confirmed these settings, demonstrating a significant improvement with surface roughness reduced by 23.08 %, tool flank and face wear exhibited a 21.97 % and 26.1 % decrease, respectively, while burr width and height reduced by 21.76 % and 25.52 %, respectively, underscoring the effectiveness of the optimized process configuration.

7. Future work

The present study provides a foundation for extending hybrid laser-assisted micromilling to a broader range of materials and operating conditions. Future investigations may explore the application of this optimized approach to other difficult-to-machine superalloys and miniaturized functional components where dimensional accuracy and surface integrity are critical. Further work could also focus on advancing towards high-speed micromilling regimes, assessing the thermal–mechanical coupling and tool–workpiece interaction at elevated speeds. In addition, multi-process hybridization such as combining laser assistance with ultrasonic or vibration-assisted micromilling under both low- and high-speed conditions, offers significant potential to enhance material removal efficiency, minimize burr formation, and improve tool life. Moreover, a dedicated comparative investigation between conventional laser-assisted micromachining and the sequential laser-hybrid micromilling approach presented in this study is recommended, to quantitatively assess the relative benefits. These directions would contribute to the broader implementation of hybrid micromachining in precision manufacturing applications.

CRediT authorship contribution statement

Ahmad Waqar Tehami: Writing – original draft, Visualization, Validation, Resources, Methodology, Investigation, Formal analysis, Data curation, Conceptualization. **Muhammad Rizwan Ul Haq:** Writing – original draft, Visualization, Validation, Supervision, Project administration, Methodology, Investigation, Formal analysis, Data curation, Conceptualization. **Muhammad Ali Khan:** Writing – original draft, Visualization, Validation, Supervision, Resources, Methodology, Investigation, Formal analysis, Data curation, Conceptualization. **Jaffery Syed Husain Imran:** Writing – original draft, Visualization, Validation, Supervision, Resources, Project administration, Methodology, Investigation, Formal analysis, Data curation, Conceptualization. **Muhammad Iftikhar Faraz:** Writing – original draft, Visualization, Validation, Project administration, Methodology, Investigation, Formal analysis, Data curation. **Jana Petru:** Writing – original draft, Visualization, Validation, Resources, Methodology, Investigation, Formal analysis, Data curation.

Institutional Review Board Statement

Not applicable

Funding

The authors extend their acknowledgement to the financial support of the European Union under the REFRESH-Research Excellence For REgion Sustainability and High-tech Industries project number CZ.10.03.01/00/22_003/0000048 via the Operational Programme Just Transition. This work was supported by the Deanship of Scientific Research, Vice Presidency for Graduate Studies and Scientific Research, King Faisal University, Saudi Arabia (Grant No. KFU254268).

Declaration of Competing Interest

The authors declare that they have no known competing financial interests or personal relationships that could have appeared to influence the work reported in this paper.

Acknowledgments

Not applicable.

Data Availability

Data will be made available on request.

References

[1] F. Schneider, J. Das, B. Kirsch, B. Linke, J.C. Aurich, Sustainability in ultra precision and micro machining: a review, Int J. Precis Eng. Manuf. Green. Technol. 6 (2019) 601–610, https://doi.org/10.1007/s40684-019-00035-2.
[2] M. Hasan, J. Zhao, Z. Jiang, Micromanufacturing of composite materials: a review, Int J. Extrem Manuf. 1 (2019), https://doi.org/10.1088/2631-7990/ab0f74.
[3] D. de Oliveira, M. Ziberov, R.L. de Paiva, M.B. da Silva, An experimental evaluation of cutting parameters influence on the surface integrity and tool wear mechanisms on the dry micromilling of austenitic alloy Inconel 718, Wear (2025) 1–11, https://doi.org/10.1016/j.wear.2025.205789.
[4] L.H. Xu, H.B. Na, G.C. Han, Machinablity improvement with ultrasonic vibration–assisted micro-milling, Adv. Mech. Eng. 10 (2018) 1–12, https://doi.org/10.1177/1687814018812531.
[5] W. Xia, X. Zhao, L. Yue, Z. Zhang, Microstructural evolution and creep mechanisms in Ni-based single crystal superalloys: a review, J. Alloy. Compd. 819 (2020) 152954, https://doi.org/10.1016/j.jallcom.2019.152954.
[6] W. Frifita, S. Ben Salem, A. Haddad, M.A. Yallese, Optimization of machining parameters in turning of Inconel 718 Nickel-base super alloy, Mech. Ind. 21 (2020), https://doi.org/10.1051/meca/2020001.

[7] Melting S.L. Modification of Inconel 718 Properties by In Situ Y Addition in Selective Laser Melting, 2022.

[8] S. Periane, A. Duchosal, S. Vaudreuil, H. Chibane, A. Morandeau, M. Anthony Xavior, et al., Influence of heat treatment on the fatigue resistance of Inconel 718 fabricated by selective laser melting (SLM), Mater. Today Proc. 46 (2021) 7860–7865, https://doi.org/10.1016/j.matpr.2021.02.447.

[9] C. Yu, Z. Huang, Z. Zhang, J. Shen, J. Wang, Z. Xu, Influence of post-processing on very high cycle fatigue resistance of Inconel 718 obtained with laser powder bed fusion, Int J. Fatigue 153 (2021) 106510, https://doi.org/10.1016/j.ijfatigue.2021.106510.

[10] B. Blakey-Milner, P. Gradl, G. Snedden, M. Brooks, J. Pitot, E. Lopez, et al., Metal additive manufacturing in aerospace: a review, Mater. Des. 209 (2021) 110008, https://doi.org/10.1016/j.matdes.2021.110008.

[11] Jain K., Tak M., Mote R.G. Impact of surface micro-dimples on machinability of Inconel 718 alloy 2025. https://doi.org/10.1063/10.0028754.

[12] H. Martins, H. Puga, Ultrasonic ASsisted Machining overview: accessing feasibility and overcoming challenges for milling applications, Metals 13 (2023), https://doi.org/10.3390/met13050908.

[13] M. Bilgin, Ş. Karabulut, H. Karakoç, Y. Kayır, M. Sarıkaya, An experimental investigation on machining-induced surface/subsurface characteristics of nickel based Inc-718 alloy: a novel hybrid approach in milling process, Tribol. Int. 191 (2024), https://doi.org/10.1016/j.triboint.2023.109120.

[14] A. Marques, B. Guimarães, F. Bartolomeu, G. Miranda, F.S. Silva, O. Carvalho, Multi-material Inconel 718 – Aluminium parts targeting aerospace applications: a suitable combination of low-weight and thermal properties, Opt. Laser Technol. 158 (2023), https://doi.org/10.1016/j.optlastec.2022.108913.

[15] N. Ngah, M.S. Kasim, H.N. Ghanesan, S.N.A. Yusof, S.B. Mohamed, Z.A. Rahman, et al., A brief review of ultrasonic assisted milling of Inconel 718, J. Tribol. 40 (2024) 14–38.

[16] E. Kaya, B. Akyüz, Effects of cutting parameters on machinability characteristics of Ni-based superalloys: a review, Open Eng. 7 (2017) 330–342, https://doi.org/10.1515/eng-2017-0037.

[17] D.M. D'Addona, S.J. Raykar, M.M. Narke, High Speed Machining of Inconel 718: Tool Wear and Surface Roughness Analysis, in: Procedia CIRP, 62, Elsevier B.V, 2017, pp. 269–274, https://doi.org/10.1016/j.procir.2017.03.004.

[18] W. Grzesik, P. Niesłony, W. Habrat, J. Sieniawski, P. Laskowski, Investigation of tool wear in the turning of Inconel 718 superalloy in terms of process performance and productivity enhancement, Tribol. Int 118 (2018) 337–346, https://doi.org/10.1016/j.triboint.2017.10.005.

[19] M.S.A. Hafiz, M.S. Kasim, W.N.F. Mohamad, R. Izamshah, M.S.A. Aziz, M. Akmal, et al., Machinability ultrasonic assisted milling of inconel 718 by using taguchi method, ARPN J. Eng. Appl. Sci. 13 (2018) 8221–8226.

[20] I. Ucun, K. Aslantasx, B. Gökcxe, F. Bedir, Effect of tool coating materials on surface roughness in micromachining of Inconel 718 super alloy, Proc. Inst. Mech. Eng. Part B J. Eng. Manuf. 228 (2014) 1550–1562, https://doi.org/10.1177/0954405414522217.

[21] Irfan Ucun, K. Aslantas, F. Bedir, An experimental investigation of the effect of coating material on tool wear in micro milling of Inconel 718 super alloy, Wear 300 (2013) 8–19, https://doi.org/10.1016/j.wear.2013.01.103.

[22] G. Mustafa, M.T. Anwar, A. Ahmed, M. Nawaz, T. Rasheed, Influence of machining parameters on machinability of Inconel 718—a review, Adv. Eng. Mater. 24 (2022) 1–17, https://doi.org/10.1002/adem.202200202.

[23] C. Nath, M. Rahman, Effect of machining parameters in ultrasonic vibration cutting, Int J. Mach. Tools Manuf. 48 (2008) 965–974, https://doi.org/10.1016/j.ijmachtools.2008.01.013.

[24] D. Finkeldei, M. Sexauer, F. Bleicher, End milling of inconel 718 using solid Si3N4 ceramic cutting tools, Procedia CIRP 81 (2019) 1131–1135, https://doi.org/10.1016/j.procir.2019.03.280.

[25] J. Díaz-álvarez, V. Criado, H. Miguélez, Luis Cantero, J. PCBN performance in high speed finishing turning of inconel 718, Metals 8 (2018), https://doi.org/10.3390/met8080582.

[26] N. Tandekar, A. Kumar, K. Valleti, Machining of Ni-based superalloys using CAPVD coated carbide tools, Mater. Today Commun. 39 (2024) 109101, https://doi.org/10.1016/j.mtcomm.2024.109101.

[27] M. Sheheryar, M.A. Khan, S.H.I. Jaffery, M. Alruqi, R. Khan, M.N. Bashir, et al., Multi-objective optimization of process parameters during micro-milling of nickel-based alloy Inconel 718 using taguchi-grey relation integrated approach, Materials 15 (2022), https://doi.org/10.3390/ma15238296.

[28] Giasin K. Effect of Tool Coating and Cutting Parameters on Surface Roughness and Burr Formation during Micromilling of Inconel 718, 2021.

[29] Faraz M.I., Petru J. Evaluation of Machining Variables on Machinability of Nickel Alloy Inconel 718 Using Coated Carbide Tools, 2024.

[30] A.K. Sahu, J. Malhotra, S. Jha, Laser-based hybrid micromachining processes: a review, Opt. Laser Technol. 146 (2022) 107554, https://doi.org/10.1016/j.optlastec.2021.107554.

[31] K. Singh, S.K. Maurya, S. Kumar, A review on introduction to hybrid machining process, Int. J. Adv. Eng. Technol. 2 (2018) 22–26.

[32] L. Zhu, Z. Yang, B. Xin, S. Wang, G. Meng, J. Ning, et al., Microstructure and mechanical properties of parts formed by ultrasonic vibration-assisted laser cladding of Inconel 718, Surf. Coat. Technol. 410 (2021), https://doi.org/10.1016/j.surfcoat.2021.126964.

[33] A. Rauf, M.A. Khan, S.H.I. Jaffery, S.I. Butt, Effects of machining parameters, ultrasonic vibrations and cooling conditions on cutting forces and tool wear in meso scale ultrasonic vibrations assisted end-milling (UVAEM) of Ti–6Al–4V under dry, flooded, MQL and cryogenic environments – a statistical, J. Mater. Res. Technol. 30 (2024) 8287–8303, https://doi.org/10.1016/j.jmrt.2024.05.202.

[34] H. Wang, L. Li, S. Zhu, Y. Xu, N. Ren, Effect of water-based ultrasonic vibration on the quality of laser trepanned microholes in nickel super-alloy workpieces, J. Mater. Process Technol. 272 (2019) 170–183, https://doi.org/10.1016/j.jmatprotec.2019.04.034.

[35] Zhao G., Zhao B., Ding W., Xin L. Nontraditional energy-assisted materials and components in aerospace community: a comparative analysis, 2024.

[36] B. Lauwers, F. Klocke, A. Klink, A.E. Tekkaya, R. Neugebauer, D. McIntosh, Hybrid processes in manufacturing, CIRP Ann. Manuf. Technol. 63 (2014) 561–583, https://doi.org/10.1016/j.cirp.2014.05.003.

[37] S. Ravi-Kumar, B. Lies, H. Lyu, H. Qin, Laser ablation of polymers: a review, Procedia Manuf. 34 (2019) 316–327, https://doi.org/10.1016/j.promfg.2019.06.155.

[38] S. Rao, A.V. Rao, D. Marla, A.A. Gokhale, S.S. Joshi, Analysis of laser-induced surface damage of single-crystal Ni-based superalloy towards improving machinability, J. Manuf. Process 118 (2024) 357–375, https://doi.org/10.1016/j.jmapro.2024.03.032.

[39] F. Hojati, B. Azarhoushang, A. Daneshi, D. Biermann, Laser pre-structure-assisted micro-milling of Ti6Al4V titanium alloy, Int J. Adv. Manuf. Technol. 120 (2022) 1765–1776, https://doi.org/10.1007/s00170-022-08774-4.

[40] Davim J.P. Nontraditional Machining Processes. n.d.

[41] C.A. McNally, J. Folkes, I.R. Pashby, Laser drilling of cooling holes in aeroengines: state of the art and future challenges, Mater. Sci. Technol. 20 (2004) 805–813, https://doi.org/10.1179/026708304225017391.

[42] J. Dutta Majumdar, I. Manna, Laser material processing, Int. Mater. Rev. 56 (2011) 341–388, https://doi.org/10.1179/1743280411Y.0000000003.

[43] L. Romoli, R. Vallini, Experimental study on the development of a micro-drilling cycle using ultrashort laser pulses, Opt. Lasers Eng. 78 (2016) 121–131, https://doi.org/10.1016/j.optlaseng.2015.10.010.

[44] Zhang H., Chen F., Li Z., Hu W., Sun T., Zhang J. Investigation of Laser-Assisted Micro-Milling Process of Inconel 718, 2023.

[45] A. Aramcharoen, P.T. Mativenga, Size effect and tool geometry in micromilling of tool steel, Precis Eng. 33 (2009) 402–407, https://doi.org/10.1016/j.precisioneng.2008.11.002.

[46] F. Brandão, D. Oliveira, A. Roger, R. Teixeira, A. Fagali, D. Souza, Size effect and minimum chip thickness in micromilling, Int. J. Mach. Tools Manuf. 89 (2015) 39–54, https://doi.org/10.1016/j.ijmachtools.2014.11.001.

[47] N.A.K. Mathew, J. Size effect and micro endmilling performance while sustainable machining on Inconel 718, Mater. Manuf. Process 36 (2021) 668–676, https://doi.org/10.1080/10426914.2020.1854465.

[48] S.H.I. Jaffery, M. Khan, L. Ali, P.T. Mativenga, Statistical analysis of process parameters in micromachining of Ti-6Al-4V alloy, Proc. Inst. Mech. Eng. Part B J. Eng. Manuf. 230 (2015) 1017–1034, https://doi.org/10.1177/0954405414564409.

[49] S.Z. Chavoshi, X. Luo, Hybrid micro-machining processes: a review, Precis Eng. 41 (2015) 1–23, https://doi.org/10.1016/j.precisioneng.2015.03.001.

[50] J. Zhao, Z. Liu, B. Wang, J. Hu, PVD AlTiN coating effects on tool-chip heat partition coefficient and cutting temperature rise in orthogonal cutting Inconel 718, Int. J. Heat. Mass Transf. 163 (2020) 120449, https://doi.org/10.1016/j.ijheatmasstransfer.2020.120449.

[51] E. Cui, J. Zhao, X. Wang, S. Song, Cutting performance, failure mechanisms and tribological properties of GNPs reinforced Al2O3/Ti(C,N) ceramic tool in high speed turning of Inconel 718, Ceram. Int. 46 (2020) 18859–18867, https://doi.org/10.1016/j.ceramint.2020.04.206.

[52] O. Pereira, A. Celaya, G. Urbikaín, A. Rodríguez, A. Fernández-Valdivielso, Noberto López de Lacalle, L. CO2 cryogenic milling of Inconel 718: cutting forces and tool wear, J. Mater. Res. Technol. 9 (2020) 8459–8468, https://doi.org/10.1016/j.jmrt.2020.05.118.

[53] A. Baig, S.H.I. Jaffery, M.A. Khan, M. Alruqi, Statistical analysis of surface roughness, burr formation and tool wear in high speed micro milling of Inconel 600 alloy under cryogenic, wet and dry conditions, Micromachines 14 (2023), https://doi.org/10.3390/mi14010013.

[54] M.K. Sinha, D. Setti, S. Ghosh, P.V. Rao, An investigation on surface burn during grinding of Inconel 718 an investigation on surface burn during grinding of Inconel 718, J. Manuf. Process 21 (2016) 124–133, https://doi.org/10.1016/j.jmapro.2015.12.004.

[55] E.O. Ezugwu, Z.M. Wang, A.R. Machado, The machinability of nickel-based alloys: A review, J. Mater. Process Technol. 86 (1998) 1–16, https://doi.org/10.1016/S0924-0136(98)00314-8.

[56] C.A. Buckner, R.M. Lafrenie, J.A. Dénommée, J.M. Caswell, D.A. Want, G.G. Gan, et al., Ultrasonic assisted machining of nickel-based superalloy Inconel 718, Intech 11 (2018) 13.

[57] Y. He, Z. Zhou, P. Zou, X. Gao, K.F. Ehmann, Study of ultrasonic vibration–assisted thread turning of Inconel 718 superalloy, Adv. Mech. Eng. 11 (2019) 1–12, https://doi.org/10.1177/1687814019883772.

[58] M.S.A. Hafiz, M.H.A. Kawaz, W.N.F. Mohamad, M.S. Kasim, R. Izamshah, J. B. Saedon, et al., A review on feasibility study of ultrasonic assisted machining on aircraft component manufacturing, IOP Conf. Ser. Mater. Sci. Eng. 270 (2017), https://doi.org/10.1088/1757-899X/270/1/012034.

[59] R. Lindvall, J.M. Bello Bermejo, A. Bjerke, J.M. Andersson, E. Vikenadler, R. M'Saoubi, et al., On the wear mechanisms of uncoated and coated carbide tools in milling titanium alloys, Int J. Refract Met Hard Mater. 124 (2024), https://doi.org/10.1016/j.ijrmhm.2024.106806.

[60] M. Takács, B. Verö, I. Mészáros, Micromilling of metallic materials, J. Mater. Process. Technol. 138 (2003) 152–155, https://doi.org/10.1016/S0924-0136(03)00064-5.

[61] S. ul hasan, S. Ali, S.H.I. Jaffery, E. ud Din, A. Mubashir, M. Khan, Study of burr width and height using ANOVA in laser hybrid micro milling of titanium alloy (Ti6Al4V), J. Mater. Res. Technol. (2022), https://doi.org/10.1016/j.jmrt.2022.11.051.

[62] J.V. Abellán-Nebot, C. Vila Pastor, H.R. Siller, A review of the factors influencing surface roughness in machining and their impact on sustainability, Sustain 16 (2024), https://doi.org/10.3390/su16051917.

[63] N. Ngah, M.S. Kasim, H.N. Ghanesan, S.N.A. Yusof, S.B. Mohamed, Z.A. Rahman, et al., A brief review of ultrasonic assisted milling of Inconel 718, J. Tribol. 40 (2024) 14–38.

[64] C. Camposeco-negrete, Optimization of cutting parameters for minimizing energy consumption in turning of AISI 6061 T6 using Taguchi methodology and ANOVA, J. Clean. Prod. (2013), https://doi.org/10.1016/j.jclepro.2013.03.049.

[65] K.N. Anand, J. Mathew, Evaluation of size effect and improvement in surface characteristics using sunflower oil-based MQL for sustainable micro-endmilling of Inconel 718, J. Braz. Soc. Mech. Sci. Eng. 42 (2020) 1–13, https://doi.org/10.1007/s40430-020-2239-0.

[66] Sankeerth A., Pagidi K., Gurabvaiah M., Chilakalapalli P., Prakasa S., Barmavatu P., et al. Laser-assisted machining of niobium alloy (C-103): effects of process parameters on cutting force and surface finish, 2025.

[67] D. Serje, J. Pacheco, E. Diez, Micromilling research: current trends and future prospects, Int. J. Adv. Manuf. Technol. 111 (2020) 1889–1916, https://doi.org/10.1007/s00170-020-06205-w.

[68] G.C. Verma, P.M. Pandey, Machining forces in ultrasonic-vibration assisted end milling, Ultrasonics 94 (2019) 350–363, https://doi.org/10.1016/j.ultras.2018.07.004.

[69] J. Zhang, Z. Zheng, Effects on vibration and surface roughness in high speed micro end-milling of Inconel 718 with minimum quantity, Lubrication (2017), https://doi.org/10.1088/1742-6596/755/1/011001.

[70] C. Zhang, Y. Qiu, F. Jiao, J. Wang, X. Wang, Research on temperature characteristics and the machining process in laser ultrasonic-assisted milling of cemented carbide, Int. J. Refract. Met. Hard Mater. 128 (2025) 1–15, https://doi.org/10.1016/j.ijrmhm.2024.107031.

[71] M.A. Rahman, M.Y. Ali, A.S. Khairuddin, Effects on Vibration and Surface Roughness in High Speed Micro End-Milling of Inconel 718 with Minimum Quantity Lubrication, in: IOP Conf. Ser. Mater. Sci. Eng., 184, Institute of Physics Publishing, 2017, https://doi.org/10.1088/1757-899X/184/1/012037.

[72] Lu X., Jia Z., Wang H., Si L., Wang X. Surface roughness prediction model of micro-milling Inconel 718 with consideration of tool wear "Surface roughness prediction model of micro-milling Inconel 718 with consideration of tool wear." vol. 12., 2016.

[73] X. Lu, Z. Jia, H. Wang, X. Hu, G. Li, L. Si, Measurement-based modelling of cutting forces in micro-milling of Inconel 718, Int. J. Nanomanuf. 13 (2017) 1–11, https://doi.org/10.1504/IJNM.2017.082406.

[74] U. Maheshwera, R. Paturi, B. VD, N.S. Reddy, Progress of machinability on the machining of Inconel 718: a comprehensive review on the perception of cleaner machining, Clean. Eng. Technol. 5 (2021) 100323, https://doi.org/10.1016/j.clet.2021.100323.

[75] M.C. Cakir, C. Ensarioglu, I. Demirayak, Mathematical modeling of surface roughness for evaluating the effects of cutting parameters and coating material, J. Mater. Process Technol. 209 (2009) 102–109, https://doi.org/10.1016/j.jmatprotec.2008.01.050.

[76] Platt T., Meijer A., Biermann D. Conduction-Based Thermally Assisted Micromilling Process for Cutting Di ffi cult-to-Machine Materials, 2020.

[77] S. Ullah, Z. Liang, Y. Du, Z. Su, C. Guo, Z. Yin, et al., Ultrasonic vibration-assisted micro-milling: A comprehensive review, 2025009–0, J. Adv. Manuf. Sci. Technol. 0 (2024), https://doi.org/10.51393/j.jamst.2025009.

[78] K.M. Li, S.Y. Chou, Experimental evaluation of minimum quantity lubrication in near micro-milling, J. Mater. Process Technol. 210 (2010) 2163–2170, https://doi.org/10.1016/j.jmatprotec.2010.07.031.

[79] X. Liang, Z. Liu, B. Wang, X. Hou, Modeling of plastic deformation induced by thermo-mechanical stresses considering tool flank wear in high-speed machining Ti-6Al-4V, Int. J. Mech. Sci. 140 (2018) 1–12, https://doi.org/10.1016/j.ijmecsci.2018.02.031.

[80] Saleh Alghamdi S., John S., Roy Choudhury N., Dutta N.K. polymers Additive Manufacturing of Polymer Materials: Progress, Promise and Challenges, 2021. https://doi.org/10.3390/polym13.

[81] M.A. Khan, S.H.I. Jaffery, M. Khan, M. Younas, S.I. Butt, R. Ahmad, et al., Multi-objective optimization of turning titanium-based alloy Ti-6Al-4V under dry, wet, and cryogenic conditions using gray relational analysis (GRA), Int. J. Adv. Manuf. Technol. 106 (2020) 3897–3911, https://doi.org/10.1007/s00170-019-04913-6.

[82] M.A. Khan, S.H.I. Jaffery, M. Khan, M. Younas, S.I. Butt, R. Ahmad, et al., Statistical analysis of energy consumption, tool wear and surface roughness in machining of titanium alloy (Ti-6Al-4V) under dry, wet and cryogenic conditions, Mech. Sci. 10 (2019) 561–573, https://doi.org/10.5194/ms-10-561-2019.

[83] E.O. Ezugwu, J. Bonney, Y. Yamane, An overview of the machinability of aeroengine alloys, J. Mater. Process Technol. 134 (2003) 233–253, https://doi.org/10.1016/S0924-0136(02)01042-7.

[84] A.G. dos Santos, D. De Oliveira, M.C. Gomes, M.J. Jackson, M.B. da Silva, Correlation between tool wear and machining temperature in micromilling of Ti-6Al-4V alloy, Wear (2025), https://doi.org/10.1016/j.wear.2025.205793.

[85] Krishnan N.A., Mathew J. Studies on wear behavior of AlTiN-coated WC tool and machined surface quality in micro endmilling of Inconel 718 n.d. https://doi.org/10.1007/s00170-020-05875-w/Published.

[86] M. Kuntoğlu, H. Sağlam, Investigation of progressive tool wear for determining of optimized machining parameters in turning, Meas. J. Int. Meas. Confed. 140 (2019) 427–436, https://doi.org/10.1016/j.measurement.2019.04.022.

[87] J. Hou, W. Zhou, H. Duan, G. Yang, H. Xu, N. Zhao, Influence of cutting speed on cutting force, flank temperature, and tool wear in end milling of Ti-6Al-4V alloy, Int. J. Adv. Manuf. Technol. 70 (2014) 1835–1845, https://doi.org/10.1007/s00170-013-5433-8.

[88] E.O. Ezugwu, Z.M. Wang, Titanium alloys and their machinability - a review, J. Mater. Process Technol. 68 (1997) 262–274, https://doi.org/10.1016/S0924-0136(96)00030-1.

[89] M. Abdul Hadi, J.A. Ghani, C.H. Che Haron, M.S. Kasim, Effect of cutting speed on the carbide cutting tool in milling Inconel 718 alloy, J. Mater. Res. 31 (2016) 1885–1892, https://doi.org/10.1557/jmr.2015.380.

[90] D. Cui, D. Zhang, B. Wu, M. Luo, An investigation of tool temperature in end milling considering the flank wear effect, Int. J. Mech. Sci. 131–132 (2017) 613–624, https://doi.org/10.1016/j.ijmecsci.2017.07.027.

[91] L. Zheng, W. Chen, D. Huo, Investigation on the tool wear suppression mechanism in non-resonant vibration-assisted micro milling, Micromachines 11 (2020), https://doi.org/10.3390/MI11040380.

[92] Y. El-Taybany, M. Hossam, J. Yan, H. El-Hofy, Surface roughness in ultrasonic-assisted and conventional milling of soda-lime glass on leave from: production engineering department, Int. J. Mach. Mach. Mater. 21 (2019) 82–99.

[93] Z. Peng, X. Zhang, D. Zhang, Performance evaluation of high-speed ultrasonic vibration cutting for improving machinability of Inconel 718 with coated carbide tools, Tribol. Int 155 (2021) 106766, https://doi.org/10.1016/j.triboint.2020.106766.

[94] Y. Cao, Y. Zhu, W. Ding, Y. Qiu, L. Wang, J. Xu, Vibration coupling effects and machining behavior of ultrasonic vibration plate device for creep-feed grinding of Inconel 718 nickel-based superalloy, Chin. J. Aeronaut. 35 (2022) 332–345, https://doi.org/10.1016/j.cja.2020.12.039.

[95] X. Jin, Y. Altintas, Prediction of micro-milling forces with finite element method, J. Mater. Process Technol. 212 (2012) 542–552, https://doi.org/10.1016/j.jmatprotec.2011.05.020.

[96] F.J.G. Silva, N.P.V. Sebbe, R.D.F.S. Costa, A.F.V. Pedroso, R.C.M. Sales-Contini, M.L.S. Barbosa, et al., Investigations on the surface integrity and wear mechanisms of TiAlYN-coated tools in Inconel 718 milling operations, Materials 17 (2024), https://doi.org/10.3390/ma17020443.

[97] M. Rakesh, S. Datta, Machining of Inconel 718 using coated WC tool: effects of cutting speed on chip morphology and mechanisms of tool wear, Arab J. Sci. Eng. 45 (2020) 797–816, https://doi.org/10.1007/s13369-019-04171-4.

[98] V.F.C. Sousa, F. Fernandes, F.J.G. Silva, R.D.F.S. Costa, N. Sebbe, R.C.M. Sales-Contini, Wear behavior phenomena of TiN/TiAlN HiPIMS PVD-coated tools on milling Inconel 718, Metals 13 (2023) 1–22, https://doi.org/10.3390/met13040684.

[99] J. Zhao, Z. Liu, Influences of coating thickness on cutting temperature for dry hard turning Inconel 718 with PVD TiAlN coated carbide tools in initial tool wear stage, J. Manuf. Process 56 (2020) 1155–1165, https://doi.org/10.1016/j.jmapro.2020.06.010.

[100] X. Kong, L. Yang, H. Zhang, K. Zhou, Y. Wang, Cutting performance and coated tool wear mechanisms in laser-assisted milling K24 nickel-based superalloy, Int. J. Adv. Manuf. Technol. 77 (2015) 2151–2163, https://doi.org/10.1007/s00170-014-6606-9.

[101] K. Mahesh, J.T. Philip, S.N. Joshi, B. Kuriachen, Machinability of Inconel 718: a critical review on the impact of cutting temperatures, Mater. Manuf. Process 36 (2021) 753–791, https://doi.org/10.1080/10426914.2020.1843671.

[102] Z. Yuan, B. Fang, Y. Zhang, F. Wang, Effect of cutting parameters on chips and burrs formation with traditional micromilling and ultrasonic vibration assisted micromilling, Int. J. Adv. Manuf. Technol. (2022) 2615–2628, https://doi.org/10.1007/s00170-021-08468-3.

[103] T. Özel, A. Olleak, T. Thepsonthi, Micro milling of titanium alloy Ti-6Al-4V: 3-D finite element modeling for prediction of chip flow and burr formation, Prod. Eng. 11 (2017) 435–444, https://doi.org/10.1007/s11740-017-0761-4.

[104] M.A. Khan, S.H.I. Jaffery, M.A. Khan, M.I. Faraz, S. Mufti, Multi-objective optimization of micro-milling titanium alloy Ti-3Al-2.5V (Grade 9) using Taguchi-grey relation integrated approach, Metals 13 (2023), https://doi.org/10.3390/met13081373.

[105] T. Platt, A. Meijer, D. Biermann, Conduction-based thermally assisted micromilling process for cutting difficult-to-machine materials, J. Manuf. Mater. Process 4 (2020), https://doi.org/10.3390/jmmp4020034.

[106] Dae Hoon K., Pil-Ho L. Experimental Study on Machinability of Ti-6Al-4V in Micro End-Milling, 2014;II:0–4.

[107] Khan M.A., Khan M.A., Aziz S., Faraz M.I., Tahir A.M., Husain S., et al. Experimental Evaluation of Surface Roughness, Burr Formation, and Tool Wear during Micro-Milling of Titanium Grade 9 (Ti-3Al-2. 5V) Using Statistical Evaluation Methods 2023.

[108] S.I. Jaffery, P.T. Mativenga, Assessment of the machinability of Ti-6Al-4V alloy using the wear map approach, Int. J. Adv. Manuf. Technol. 40 (2009) 687–696, https://doi.org/10.1007/s00170-008-1393-9.

[109] B.N. Pathak, K.L. Sahoo, M. Mishra, Effect of machining parameters on cutting forces and surface roughness in Al-(1-2) Fe-1V-1Si alloys, Mater. Manuf. Process 28 (2013) 463–469, https://doi.org/10.1080/10426914.2013.763952.

[110] R.B. Da Silva, Á.R. MacHado, E.O. Ezugwu, J. Bonney, W.F. Sales, Tool life and wear mechanisms in high speed machining of Ti-6Al-4V alloy with PCD tools under various coolant pressures, J. Mater. Process Technol. 213 (2013) 1459–1464, https://doi.org/10.1016/j.jmatprotec.2013.03.008.

[111] G. Ul Rehman, S. Husain Imran Jaffery, M. Khan, L. Ali, A. Khan, S. Ikramullah Butt, Analysis of burr formation in low speed micro-milling of titanium alloy (Ti-6Al-4V), Mech. Sci. 9 (2018) 231–243, https://doi.org/10.5194/ms-9-231-2018.
[112] Y. Yang, X. Wei, Z. Long, C. Song, C. Xie, J. Lin, The Grey-Taguchi method analysis for processing parameters optimization and experimental assessment of 42CrMo steel treated by ultrasonic surface rolling, J. Mater. Res. Technol. 23 (2023) 6244–6261, https://doi.org/10.1016/j.jmrt.2023.02.217.
[113] S. Singh, M. Doddamani, S. Powar, Multi-objective optimization of machining parameter in laser drilling of glass microballoon/epoxy syntactic foams, J. Mater. Res. Technol. 23 (2023) 3869–3879, https://doi.org/10.1016/j.jmrt.2023.02.025.
[114] S. Senthil Kumar, T.S. Senthilkumar, P. Pitchipoo, Y.D. Dwivedi, N. Nagaprasad, K. K Saxena, et al., Grey relational analysis and surface texture analysis of Al-based metal matrix composites, J. Mater. Res. Technol. 24 (2023) 5372–5388, https://doi.org/10.1016/j.jmrt.2023.04.118.
[115] J.S. Solheid, A. Elkaseer, T. Wunsch, S. Scholz, H.J. Seifert, W. Pfleging, Multiobjective optimization of laser polishing of additively manufactured Ti-6Al-4V parts for minimum surface roughness and heat-affected zone, Materials 15 (2022), https://doi.org/10.3390/ma15093323.
[116] H. Singh, P. Patrange, P. Saxena, Y.M. Puri, Multi-objective optimization of the process parameters in electric discharge machining of 316L porous stainless steel using metaheuristic techniques, Materials 15 (2022), https://doi.org/10.3390/ma15196571.
[117] D. Julong, Introduction to grey system, J. Grey Syst. 1 (1989) 1–24.
[118] E. Kuram, B. Ozcelik, Multi-objective optimization using Taguchi based grey relational analysis for micro-milling of Al 7075 material with ball nose end mill, Meas. J. Int. Meas. Confed. 46 (2013) 1849–1864, https://doi.org/10.1016/j.measurement.2013.02.002.
[119] M. Younas, S.H.I. Jaffery, M. Khan, M.A. Khan, R. Ahmad, A. Mubashar, et al., Multi-objective optimization for sustainable turning Ti6Al4V alloy using grey relational analysis (GRA) based on analytic hierarchy process (AHP), Int. J. Adv. Manuf. Technol. 105 (2019) 1175–1188, https://doi.org/10.1007/s00170-019-04299-5.
[120] S.S. Warsi, M.H. Agha, R. Ahmad, S.H.I. Jaffery, M. Khan, Sustainable turning using multi-objective optimization: a study of Al 6061 T6 at high cutting speeds, Int. J. Adv. Manuf. Technol. 100 (2019) 843–855, https://doi.org/10.1007/s00170-018-2759-2.
[121] S. Dmitrović, I. Pajčin, N. Lukić, V. Vlajkov, M. Grahovac, J. Grahovac, et al., Taguchi grey relational analysis for multi-response optimization of bacillus bacteria flocculation recovery from fermented broth by chitosan to enhance biocontrol efficiency, Polymers 14 (2022), https://doi.org/10.3390/polym14163282.